Russian Academy of sciences
Petersburg nuclear physics institute

Preprint 2104

D.V.Balin, M.J.Borkowski, V.P.Chizhov, G.A.Kolomensky, E.M.Maev, D.M.Seliverstov, G.G.Semenchuk, Yu.V.Smirenin, A.A.Vasiliev, A.A.Vorobyov, N.Yu.Zaitsev

COMPTON SCATTERING ON PROTONS: PROJECT OF EXPERIMENTAL DETERMINATION OF ELECTRIC AND MAGNETIC POLARIZABILITIES OF THE PROTON

Gatchina 1996

Abstract

A new method is proposed for experimental determination of energy dependence of the differential cross section of elastic γp scattering in the energy range of photons (20–120)MeV with $\leq$1% precision in relative measurements. Such measurements should provide in a model-independent way the electric and magnetic polarizabilities of the proton with errors of $\leq 0.5\times10^{-4} fm^3$. This accuracy can be achieved with untagged bremsstrahlung γ-quanta produced by a $\simeq$130MeV, $\simeq 10\mu A$ continuous electron beam in several hundred hours of beam time. The method provides effective rejection of the background reactions by coincident detection of the scattered photon and the recoiled proton. The scattered photons will be detected and their energy measured with a large NaI(Tl) total absorption spectrometer with intrinsic resolution of a few percents. The energy of the recoiled protons will be measured in a special high pressure (100 bar) hydrogen ionization chamber, that serves also as a target ($\simeq 3\times10^{22}$ protons/cm^2). The shape of the incident photons spectrum will be determined with the same NaI(Tl) spectrometer by detecting the events of elastic scattering on free electrons.

I. Introduction

Study of (γ,p)-scattering allows, in principle, to determine precisely [1] the generalized constants of the proton electric ($\overline{\alpha}$) and magnetic ($\overline{\beta}$) polarizabilities, defined as

$$\overline{\alpha} = 2 \sum_{n \neq N} \frac{\mid \langle n \mid D_z \mid N \rangle \mid^2}{E_n - E_N} + \Delta\alpha \equiv \alpha_0 + \Delta\alpha, \tag{1}$$

$$\overline{\beta} = 2 \sum_{n \neq N} \frac{\mid \langle n \mid M_z \mid N \rangle \mid^2}{E_n - E_N} + \Delta\beta \equiv \beta_0 + \Delta\beta. \tag{2}$$

Here α_0 and β_0 are the "static" polarizabilities; D_z and M_z are the quantum field operators of projections of the induced electric and magnetic dipole moments onto z-axis; summation is over all possible intermediate energy states E_n; E_N is the ground state energy. The correction terms $\Delta\alpha$ and $\Delta\beta$ are due to mainly non-zero charge and non-zero size (retardation effects) of the proton. According to [2,3],

$$\Delta\alpha = \frac{e^2}{3m_p}\langle r^2 \rangle + \frac{e^2}{4m_p^3}(1 + k_p^2)\,, \tag{3}$$

$$\Delta\beta = -\frac{e^2}{3m_p}\langle r^2 \rangle - \frac{e^2}{2m_p^3}(1 + k_p + k_p^2)\,, \tag{4}$$

where e, m_p, $\langle r^2 \rangle$, and k_p are the charge, mass, mean square radius, and Pauli anomalous magnetic moment of the proton, respectively.

The values of $\overline{\alpha}$ and $\overline{\beta}$ can be evaluated in a model-independent way by fitting the experimental differential cross sections (measured at the photon energies ω much smaller than the pion mass) with the theoretical differential cross sections based on the low energy theorem (LET) for Compton scattering amplitude expanded to the second order over ω.

According to [1]

$$\frac{d\sigma(\omega,\theta)}{d\Omega} = \left[\frac{d\sigma(\omega,\theta)}{d\Omega}\right]_{point} - \rho + 0(\omega^4)\,,$$

$$\begin{aligned} \rho \;=\; & \frac{e^2}{4\pi m_p}\left(\frac{\omega'}{\omega}\right)^2 (\omega\omega') \times \\ \times\; & \left[\frac{\overline{\alpha}+\overline{\beta}}{2}\,(1+cos\theta)^2 + \frac{\overline{\alpha}-\overline{\beta}}{2}\,(1-cos\theta)^2\right], \end{aligned} \qquad (5)$$

where $[d\sigma\,(\omega,\theta)\,/d\Omega]_{point}$ is exact Powell cross section for the point-like proton with the anomalous magnetic moment [4], ρ is the structure term, where ω and ω' are the energies of the incident and scattered photons, respectively, θ is the lab scattering angle, and $0(\omega^4)$ are the neglected terms of higher order structure constants.

The sum $\overline{\alpha}+\overline{\beta}$ is also constrained by the dispersion sum rule [5]:

$$\overline{\alpha}+\overline{\beta} = \frac{1}{2\pi^2}\int_0^\infty \frac{d\omega}{\omega^2}\sigma_{tot}\,(\omega) = (14.2 \pm 0.3) \times 10^{-4} fm^3, \quad (6)$$

where $\sigma_{tot}\,(\omega)$ is the total γp cross section. The integral is evaluated using the experimental data on σ_{tot} for photon energies up to 30GeV with a theoretical ansatz for higher energies. (However indicated error is certainly too small).

The contribution of the structure term ρ to the LET-formula (5) is illustrated in Fig.1. The dotted lines are $[d\sigma\,(\omega,\theta)\,/d\Omega]_{point}$, the solid lines are $d\sigma\,(\omega,\theta)\,/d\Omega$ calculated for several values of $\overline{\alpha}$ from $\overline{\alpha}$=9.2 (upper curves) to $\overline{\alpha}$=17.2 (lower curves) with a step $\delta\overline{\alpha} = 1.6$. The sum $\overline{\alpha}+\overline{\beta}$ is fixed to 14.2 (here and further $\overline{\alpha}$ and $\overline{\beta}$ are defined in units of $10^{-4} fm^3$). Fig.1 shows also the recent (Urbana, 1991) experimental data [6].

The LET-formula describes the γp-scattering with high precision at low energies. However, the sensitivity of the differential cross section to $\overline{\alpha}$ and $\overline{\beta}$ is small at such energies as one can see from Fig.1.

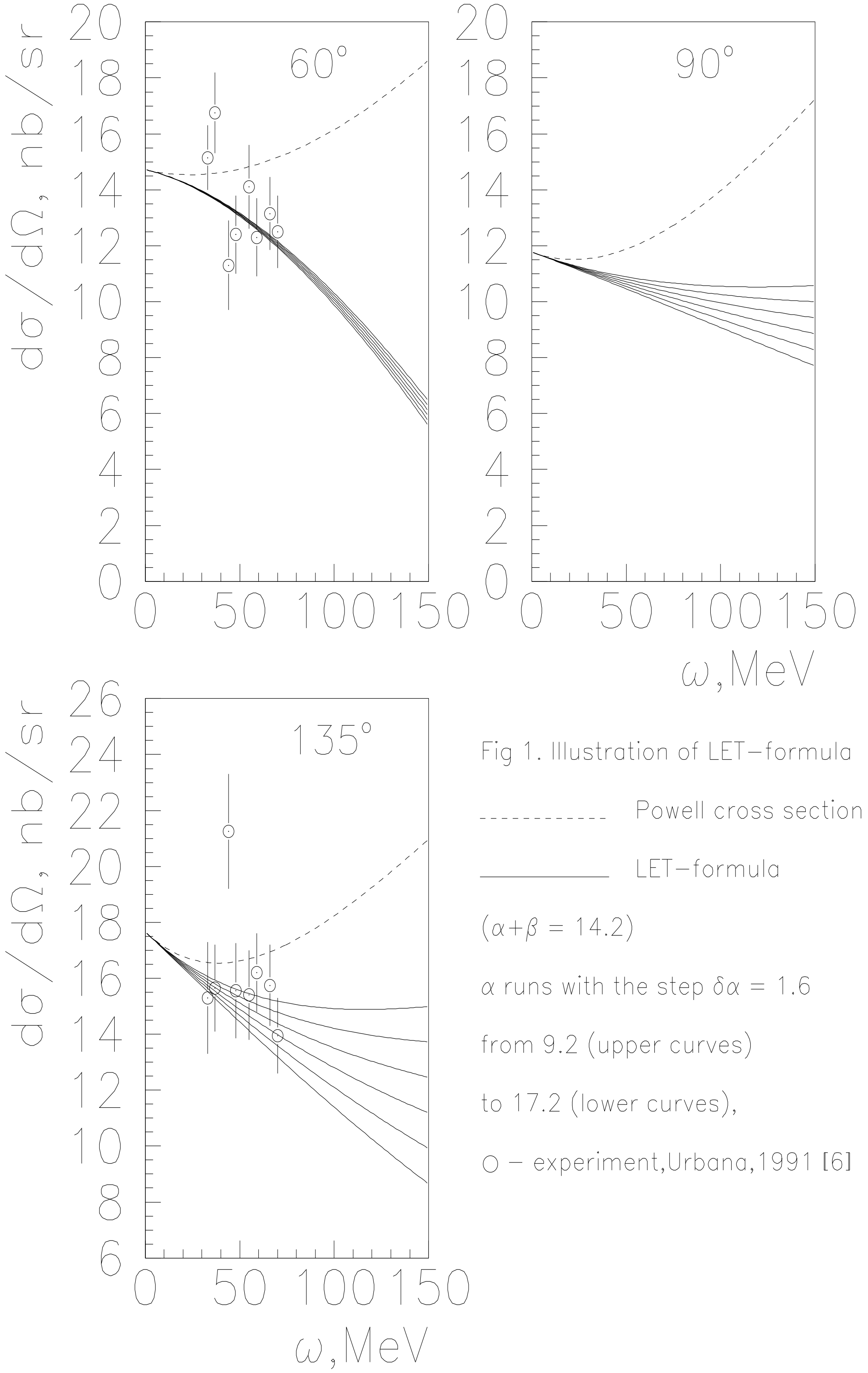

Fig 1. Illustration of LET−formula

- - - - - - - - - - - Powell cross section

———————— LET−formula

($\alpha+\beta$ = 14.2)

α runs with the step $\delta\alpha$ = 1.6

from 9.2 (upper curves)

to 17.2 (lower curves),

○ − experiment,Urbana,1991 [6]

On the other hand, extention of the measurements to higher energies may induce some uncertainties in interpretation of the experimental data caused by contribution of the $0(\omega^4)$ term in (5). There exists a theoretical model-dependent approach (MDA) [7] that aims to describe the γp-scattering up to the photon energies comparable to the pion mass. However, its precision at higher energies is not so clear. In our experiment we are not going to rely on the MDA. Instead, we intend to determine the contribution of the $0(\omega^4)$ term experimentally by measuring with high precision the energy dependence of the differential cross-sections.

The MDA fit to the published up to 1980 experimental data on γp-scattering at energies up to 400MeV shows [7], that the proton polarizabilities are in the range of

$$\overline{\alpha} \approx 10 \div 15 \; ; \;\; \overline{\beta} \approx 4 \div -1 \;\; .$$

The lowest errors were reported in the Moscow experiment [8] (1974; $\omega = 70 - 110$ MeV, $\theta = 90^0$ and 150^0):

$$\overline{\alpha} = 10.7 \pm 1.1 \; ; \quad \overline{\beta} = -0.7 \pm 1.6.$$

Note that these results were obtained using the LET-formula (with $\overline{\alpha} + \overline{\beta}$ not fixed). More recent fits of this data [9] with MDA gave the following results: $\overline{\alpha} = 11.2 \mp 1.3 \; ; \;\; \overline{\beta} = -5.2 \pm 1.6$. But the problem is that the sum $\overline{\alpha} + \overline{\beta} = 6$ is inconsistent with the experimental sum rule value of 14.2 ± 0.3.

The fit with the LET-formula to the recent (Urbana, 1991) experimental data [6] shown in Fig.1 gives

$$\overline{\alpha} = 10.6 \mp 2.2 \mp 1.4 \, ; \quad \overline{\beta} = 3.6 \pm 2.2 \pm 1.4 \quad (\overline{\alpha} + \overline{\beta} = 14.2 \;\; \text{fixed}) \; ,$$

$$\overline{\alpha} = 9.8 \mp 2.7 \mp 1.9 \, ; \quad \overline{\beta} = 2.5 \pm 3.2 \pm 0.4 \;\; (\overline{\alpha} + \overline{\beta} \;\; \text{is not fixed}).$$

Here and further the first quoted error is statistical, the second is systematic.

The MDA-fit to the experimental data of the Mainz group[10] (1992, $\varpi = 98$MeV and 132MeV, $\theta = 180^0$) provides:

$$\alpha - \beta = 7.0 \mp 2.4 \mp 2.1.$$

Assuming $\overline{\alpha} + \overline{\beta} = 14.2$ one obtains

$$\overline{\alpha} = 10.6 \mp 1.2 \mp 1.0$$

$$\overline{\beta} = 3.6 \pm 1.2 \pm 1.0 \ .$$

The latest results from Saskatoon[11] (1993, 136MeV $\leq \omega \leq 289 MeV$, $25^0 < \theta < 135^0$, MDA-fit) lead to:

$$\overline{\alpha} - \overline{\beta} = 5.5 \mp 0.7 \mp 2.1$$

and assuming $\overline{\alpha} + \overline{\beta} = 14.2$:

$$\overline{\alpha} = 9.8 \mp 0.4 \mp 1.1,$$

$$\overline{\beta} = 4.4 \pm 0.4 \pm 1.1 \ .$$

However, the errors given here do not include theoretical uncertainties of the analysis. They are estimated as $\pm(0.3 - 0.4)$ and $\pm(1.5 - 2.0)$ for the results from Mainz and Saskatoon, respectively, [12].

Thus amongst the latest experiments there is only one [6] that provides independently measured $\overline{\alpha}$ and $\overline{\beta}$, but these data are not very precise. An essential improvement of the data on the proton polarizabilities is important for tests of various nucleon models. It is needed also for extraction of the neutron polarizabilities from the data on elastic and inelastic scattering of photons by deuterons.

II. Experimental method

Our goal is to measure both $\overline{\alpha}$ and $\overline{\beta}$ with total errors $\delta\overline{\alpha} \simeq \delta\overline{\beta} \leq 0.5$. To achieve this goal we are going to measure the energy dependence of the differential γp-scattering cross sections $d\sigma_{\gamma p}(\omega, \theta_\gamma)/d\Omega$ with high relative precision in the ω-range of (20-100)MeV. The measurements will be performed at θ_γ=60^0 and θ_γ=135^0. The measured differential cross sections will be fitted with the LET-formula, in which the contribution of $0(\omega^4)$-term is parametrized as $\mathrm{b}(\theta)\times\omega^4$ (and maybe by another expression, in which the contribution of $0(\omega^{n>4})$-terms will be foreseen). From these fits the values of $\overline{\alpha}$ and $\overline{\beta}$ will be determined as well as the contribution of the $0(\omega^4)$-term.

The experiment can be done using a non-tagged bremsstrahlung γ-beam produced by a continious electron beam of $\sim$130MeV energy and of a few μA current. The photons scattered on a special hydrogen target will be detected with a large-volume total absorption γ-spectrometer with a solid angle of about $0.025sr$. However, the measurements of ω' with the γ-spectrometer alone are not enough for clean separation of the Compton scattering events from the background. There are various sources of such background. For example, an important background reaction is production of electron-positron pairs in the electric field of the proton followed by bremsstrahlung quanta emitted by the electrons (positrons) in the same field (see Appendix). There is also background from outside the target. To avoid these problems, we propose to detect the recoiled proton in addition to the scattered photon. This will be done using a high pressure hydrogen filled Ionization Chamber (IC) which serves as a target and as a recoiled proton detector at the same time. The recoils will be detected in the energy range 0.4MeV$\leq E_p \leq$8MeV. Their energy will be measured, and the $(E_p - \omega')$ correlations will be used to select clean Compton scattering events. It is essential that the IC provides practically 100% detection efficiency for the recoiled protons in the chosen energy range. Note that the lower limit of 0.4MeV in the recoils energies (set by the signal/noise ratio in the IC) determines the lowest energy of useful incident photons to be around 20MeV.

The scheme of the experiment is shown in Fig. 2. The collimated and cleaned bremsstrahlung beam passes through the hydrogen-filled IC which detects the recoiled protons. The photons scattered at the angle θ_γ are detected with the γ-spectrometer. The solid angle of the spectrometer $(0.025sr)$ is defined by a collimator. The proton density in the IC is about 3×10^{22}p/cm^2.

The whole spectrum of the γ-spectrometer $N(\omega'')$, where ω'' is the amplitude of a spectrometer signal expressed in energy units, will be subdivided into several (10$\div$15) intervals $\Delta\omega''_i$. The yield of the γp-scattering events $Y_{\gamma p}(i, \overline{\theta}_\gamma) \mid_{\omega''_i}^{\omega''_{i+1}}$ in the intervals $\Delta\omega''_i$ will be measured, the differential cross-sections $\langle d\sigma(\omega, \overline{\theta}_\gamma)/d\Omega\rangle_i$ averaged over the intervals $\Delta\omega''_i$ will be determined from the integral expression

$$\begin{aligned} Y_{\gamma p}(i, \overline{\theta}_\gamma) \mid_{\omega''_i}^{\omega''_{i+1}} &= K_1 \int_{\omega_i}^{\omega_{max}} \frac{dN(\omega, \omega_{max})}{d\omega} \frac{d\sigma(\omega, \overline{\theta}_\gamma)}{d\Omega} \times \\ &\times \; P(i, \omega') d\omega \ , \end{aligned} \tag{7}$$

where K_1 is a normalization factor that takes into account the target thickness, the solid angle of the γ-detector, the efficiency of the IC for detection of the recoiled protons. For the analysis it is important that dependences of these factors on ω are insignificant; $dN(\omega, \omega_{max})/d\omega$ is the spectrum of the incident photons;

$$P(i, \omega') = \int_{\omega''_i}^{\omega''_{i+1}} \frac{dn(\omega'', \omega')}{d\omega''} d\omega''$$

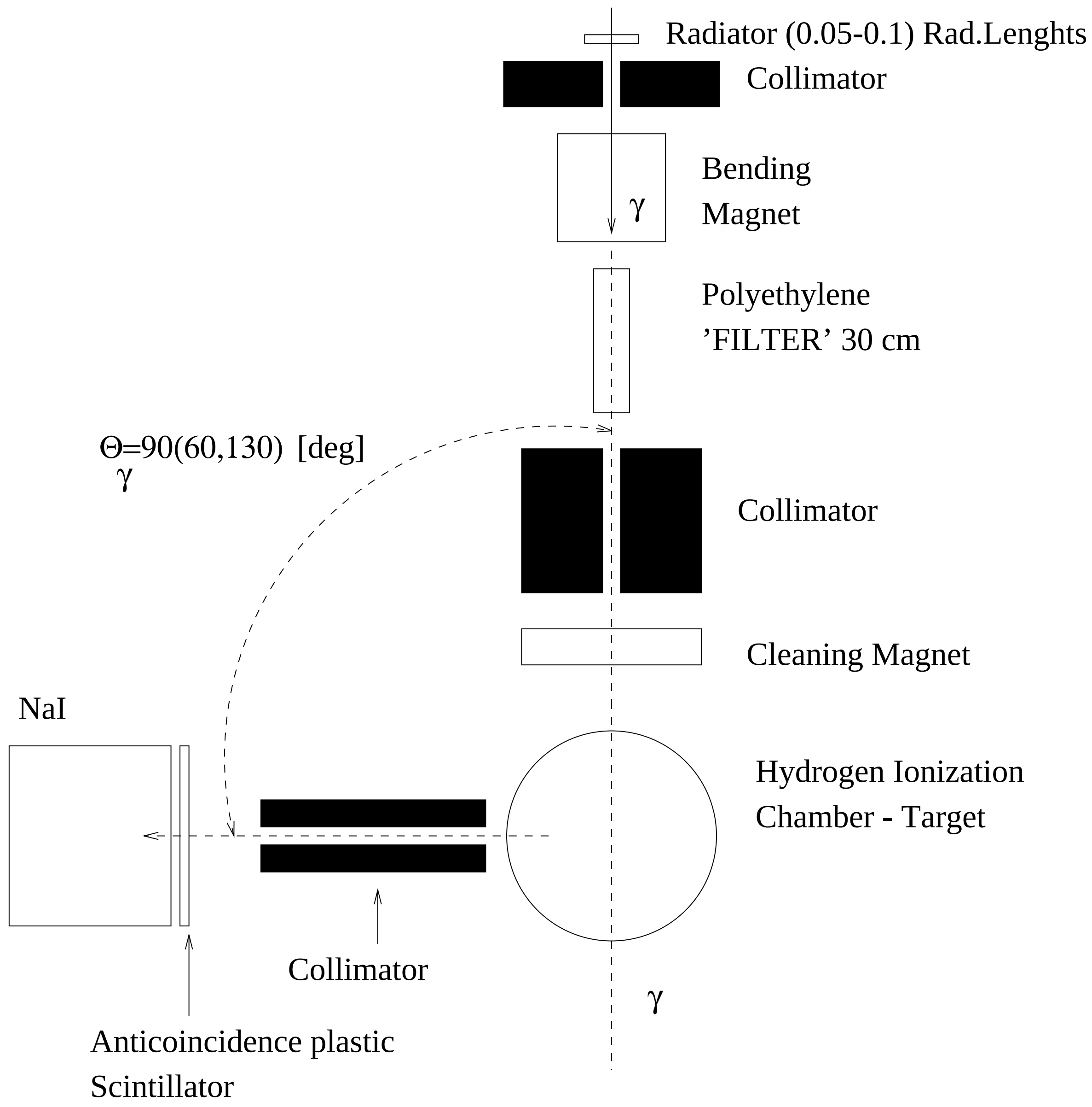

Fig.2 Plan view of the experimental layout (γp-scattering).

is the probability of registration of the scattered photons with energy ω' in the amplitude interval $\Delta\omega''_i$, and

$$dn(\omega'', \omega')/d\omega'' \equiv F(\omega'', \omega')$$

is the response function of the γ-spectrometer. F(ω'', ω') will be determined experimentally in a separate measurement.

The quantities $\langle dN(\omega, \omega_{max})/d\omega\rangle_i$ averaged over $\Delta\omega''_i$ will be determined in measurements of γe-scattering (Fig.3) using the same γ-spectrometer. The scattering angle $\overline{\theta}^e_\gamma$ will be fixed by the conditions:

$$(\omega')_{\gamma e} = (\omega')_{\gamma p} \ \text{ or}$$
$$1/m_p(1 - cos\overline{\theta}_\gamma) = 1/m_e(1 - cos\overline{\theta}^e_\gamma) \ .$$

In our case it makes $\overline{\theta}^e_\gamma = 1.337^0$ and 2.471^0 corresponding to $\overline{\theta}_\gamma = 60^0$ and 135^0, respectively. The yield of the γe-scattering events will be

$$\begin{aligned} Y_{\gamma e}(i, \overline{\theta}^e_\gamma) \mid^{\omega''_{i+1}}_{\omega''_i} &= K_2 \int_{\omega_i}^{\omega_{max}} \frac{dN(\omega, \omega_{max})}{d\omega} \\ &\times \left[\frac{d\sigma_{\gamma e}(\omega, \overline{\theta}^e_\gamma)}{d\Omega}\right]_{theory} P(i, \omega')d\omega \ , \quad (8) \end{aligned}$$

where K_2 is a normalization factor that should not depend noticeably on the energy ω, and $[d\sigma_{\gamma e}(\omega, \overline{\theta}^e_\gamma)/d\Omega]_{theory}$ is a well known quantity. In fitting (7) and (8) with the known formulae, the constants K_1, K_2, $\overline{\alpha}$, $\overline{\beta}$, $b(\overline{\theta}_{\gamma 1})$ and $b(\overline{\theta}_{\gamma 2})$ will be used as free parameters.

The preliminary results of simulation of the experiment show that we need to register some 10^6 of $\gamma + p \rightarrow \gamma' + p'$ events. This will provide statistical errors in determination of $\overline{\alpha}$ and $\overline{\beta}$ on a level of $\pm(0.3 \div 0.4)$.

In Fig.4 we show the result of fitting by the LET-formula with four free parameters $[\overline{\alpha}, \overline{\beta}, b_1(\theta_{\gamma 1}), b_2(\theta_{\gamma 2})]$ of a Monte-Carlo simulated experiment with the incident bremsstrahlung ($E_{\gamma max} = 130$MeV) beam

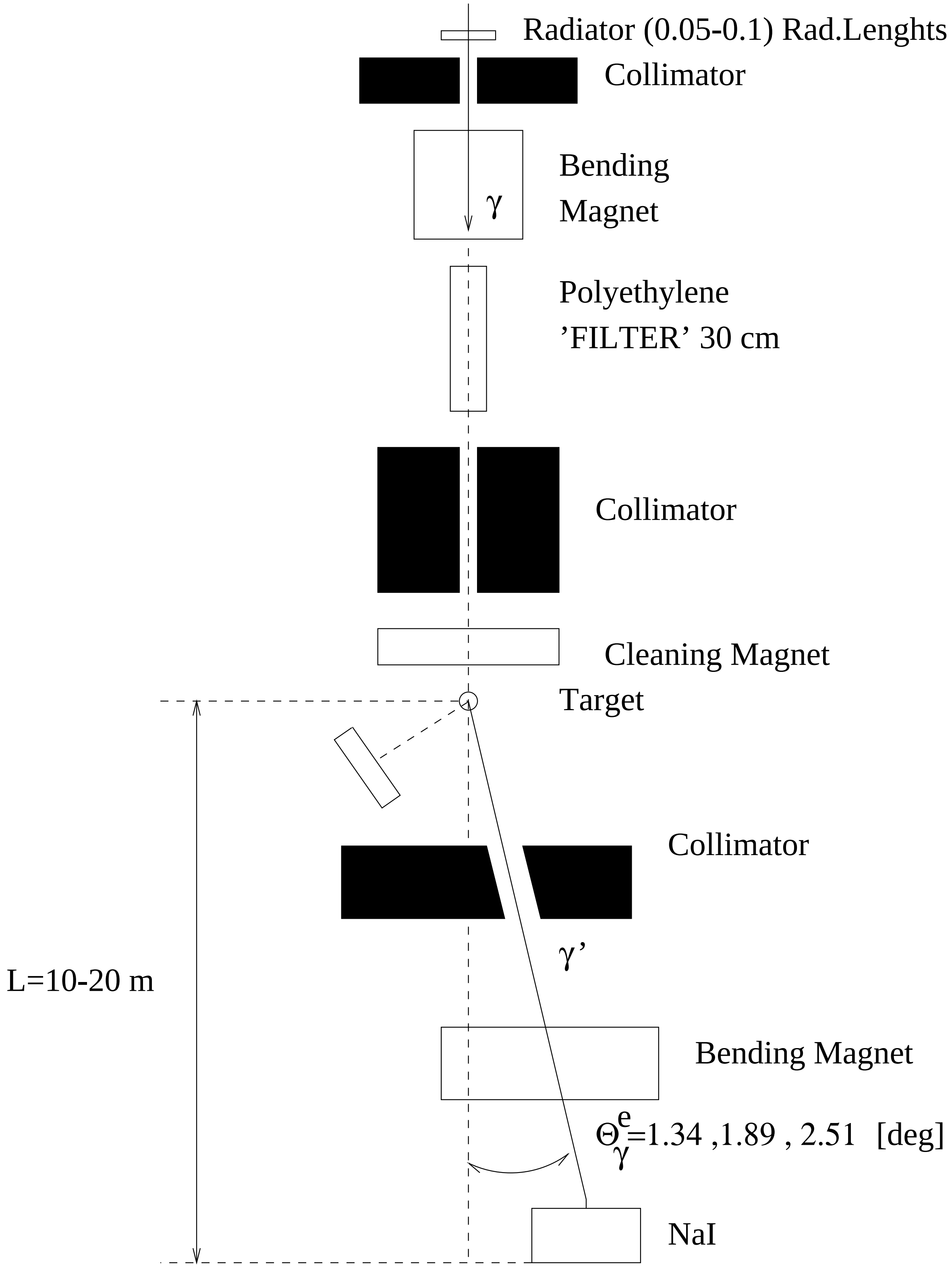

Fig.3 Plan view of the experimental layout (γe-scattering).

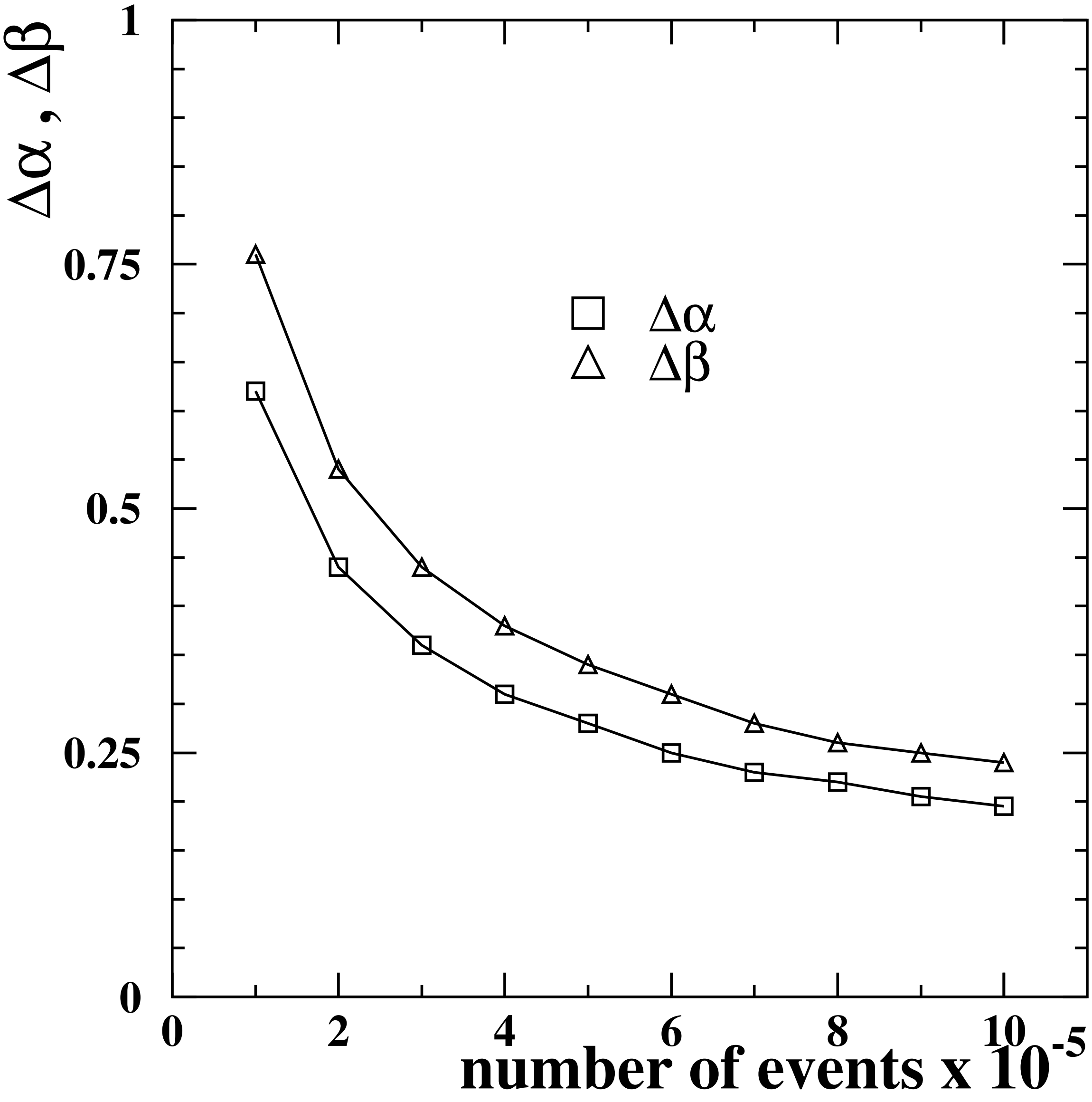

Fig.4 Statistical errors $\delta\overline{\alpha}$ and $\delta\overline{\beta}$ in function of the number of detected scattering events at each of the two scattering angles $\theta_\gamma = 60^0$ and $\theta_\gamma = 135^0$. The calculations were performed with four free parameters: $\overline{\alpha}, \overline{\beta}, b_1(\theta_{\gamma\,1)}, b_2(\theta_{\gamma\,2})$.

scattered to $\theta_{\gamma_1} = 60^0$ and $\theta_{\gamma_2} = 135^0$. Here $\delta\overline{\alpha}$ and $\delta\overline{\beta}$ are the statistical errors of the parameters $\overline{\alpha}$ and $\overline{\beta}$ depending on the number of simulated scattering events for each angle.

Below we shall consider possible systematic errors in determination of these constants.

III. Ionization chamber (IC).

The physical properties of the hydrogen-filled IC operating in the electron collection mode at gas pressure in the range from 10 to 160 bar are well-known from the experience at the Petersburg Nuclear Physics Institute (PNPI) [13]. Moreover, a special multianode IC was created [14] for detection of short-range charged particles in the presence of intense background of long-range electrons.

The scheme of the proposed IC (100 bar, 3 $\times 10^{22}$ protons/cm^2) and some parameters of the anode signals are given in Fig.5. In order to keep the background originated by the Compton recoil electrons and the e^+e^--pairs at acceptable level, the anode of the IC is divided into twenty 2.5mm wide strips separated by 0.1mm gaps. The anode strips are directed along the tracks of the recoiled protons. The kinematics of the reaction $\gamma + p \rightarrow \gamma' + p'$ in the investigated range of the photon energies is such that for fixed scattering angle $\theta_\gamma \pm \Delta\theta_\gamma$ the emission angle of the recoil protons $\theta_p(E_p) \pm \Delta\theta_p(E_p)$ practically does not depend on the photon energy E_γ (Fig.6), while $\Delta\theta_p \simeq (1/2)\Delta\theta_\gamma$. The value $\Delta\theta_\gamma = \Delta\varphi_\gamma$ is $\pm 5^0$, for the chosen solid angle of the γ-spectrometer $\Delta\Omega$=0.025sr.. Note that the reaction plane is parallel to the planes of the IC electrodes. For photon energies (30–120)MeV, (20–90)MeV and (15–70)MeV and for scattering angles 60^0, 90^0, and 130^0, respectively, the recoil proton energies are (0.4–8.2)MeV. The ranges of these recoil protons in hydrogen at the pressure of 100 bar

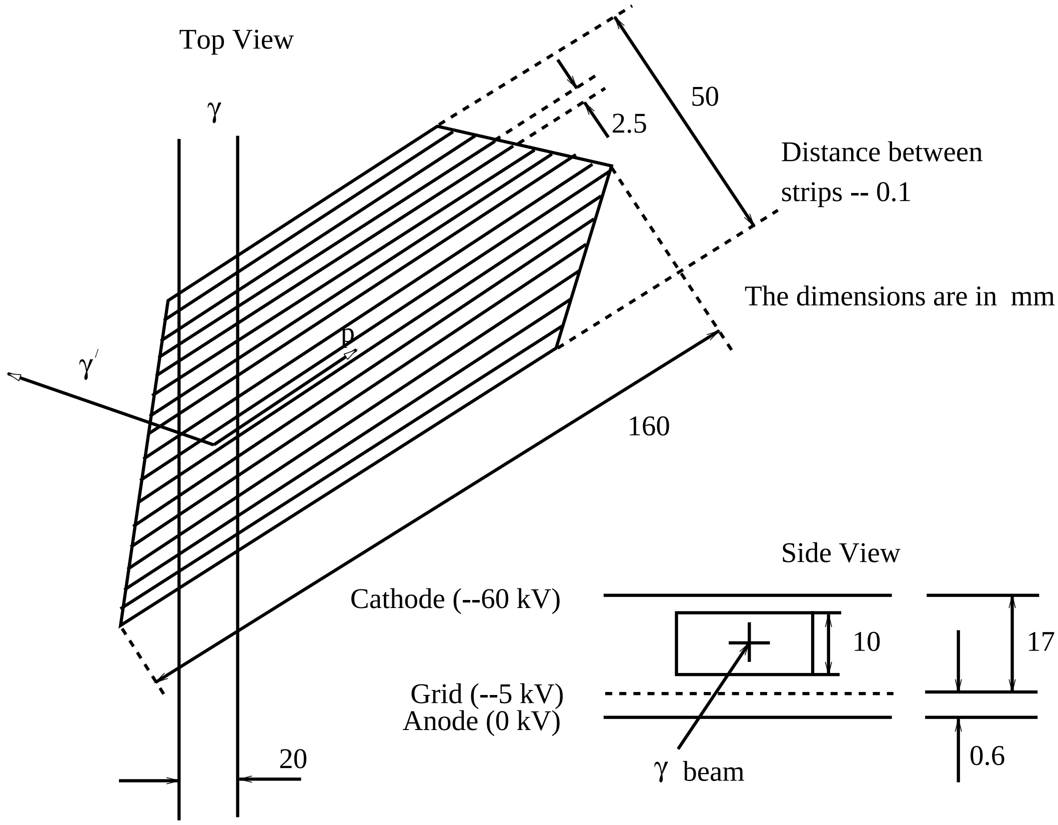

Fig.5 Layout of the ionization chamber electrodes.
p=100 bar E=32kV/cm

The ranges of protons	R_p =0.25mm - 40mm
The energies of protons	E_p =0.4MeV - 8MeV
The drift velosity	v_{drift} =0.5mm/100ns
The duration and amplitude of signals	Δt_{min} =80ns i_0 =(0.42-8)MeV/80ns
	Δt_{max} =(100-800)ns i_0 = (0.4-1)MeV/100ns

The drift time of the electron component track from cathode to anode is about 2μs.

The energies of γ-rays ω: 15-70MeV $\theta = 130^0$
20-90MeV $\theta = 90^0$
30-120MeV $\theta = 60^0$

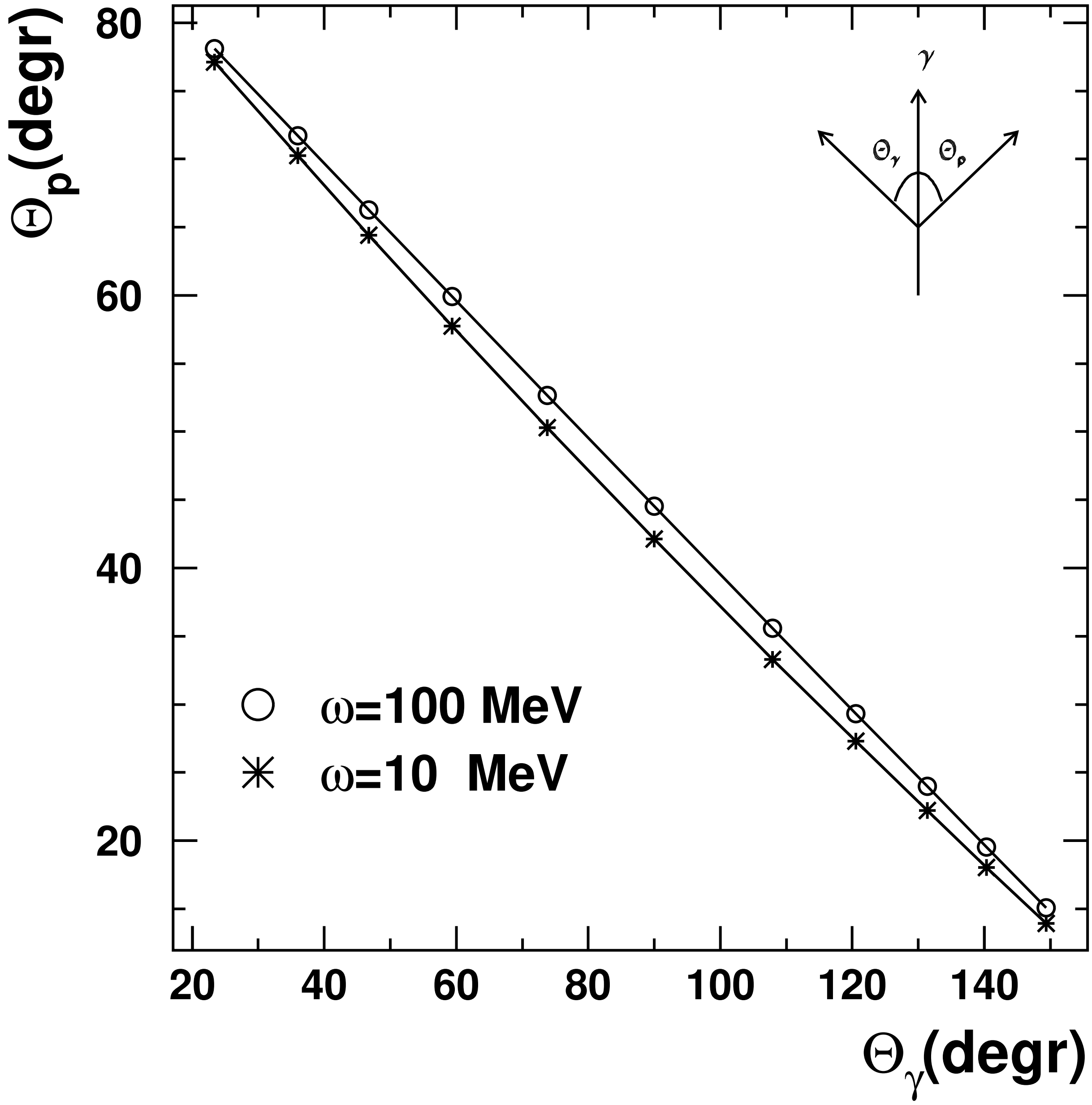

Fig.6 Recoil-proton angle θ_p *versus* photon scattering angle θ_γ for two energies of incident photons, ω.

are (0.25–40)mm. The projections of the recoil proton tracks to the anode plane overlap only one or two strips while the ionization produced by the background electrons is subdivided between many anode strips. So the ratio of the background signal to the useful one is reduced. The shape of current of the anode signals is to be analysed over a period of time from the moment of a trigger pulse up to the time of drift of the most remote tracks in the sensitive volume of the IC, T$\sim$4μs, to the anode plane, by means of flash ADCs scanning the current in 10ns bins, i(t$_i$).

The maximum length of a projection of a track on the direction perpendicular to the anode plane for $\varphi_\gamma = 5^0$ is $R_{max}\times\sin(\varphi_\gamma) \simeq$ 3.5mm. For vertical size of the incident γ-ray beam of 10mm, the minimum distance between the cathode and the grid should be 17mm. The distance between the anode and the grid is equal to 0.5mm. The minimum pulse duration (for tracks parallel to the anode plane) Δt_{min} is 80ns, and amplitudes of current signals (in energy units) are (0.34-6.5)MeV/80ns; the maximum pulse durations Δt_{max} are (100-800)ns, and maximum amplitudes are (0.32-0.8)MeV/100ns. (Recombination coefficient is $k \simeq 0.8$ at 100 bar pressure and the electrical field of 25kV/cm). In Figs.7,8 the preliminary design of the IC is shown. There are three possible directions of the IC strips with respect to the direction of the incident photons ($a_1 \to b_1$, $a_2 \to b_2$, $a_3 \to b_3$). The IC will have the inlet and outlet beryllium windows, 3mm thick, ($a_1 - a_3$, $b_1 - b_3$) 30cm away from the IC center to minimize the flux of neutrons from the Be(γ, n)-reaction. The electrons (positrons) produced in the input window will be deflected from the photon beam direction by a cleaning magnet (Fig.2). The beryllium window for scattered photons is about 5mm thick. The total IC volume is 1.5 litre (P$\times$V$\simeq$150 bar$\times$litre).

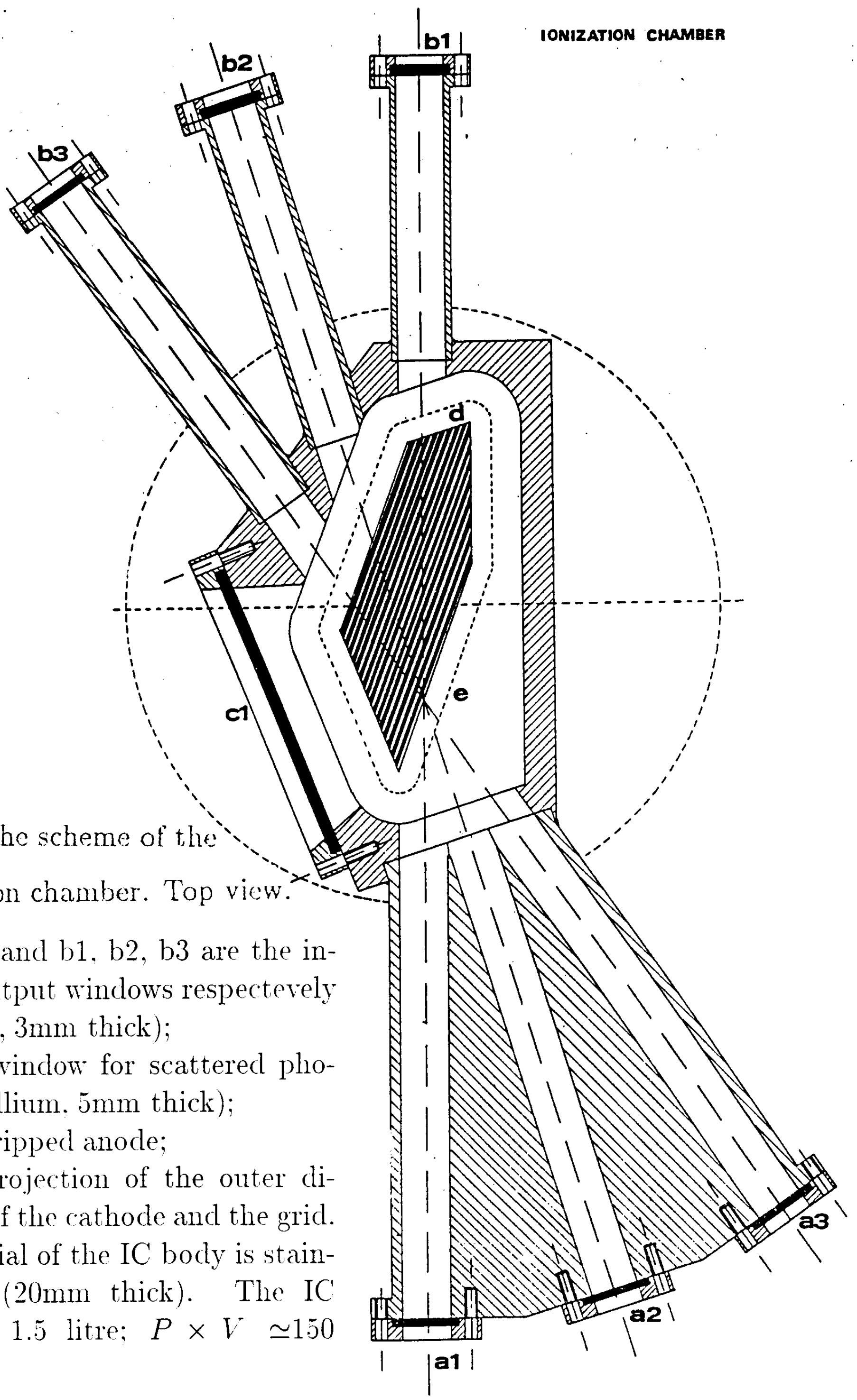

Fig.7 The scheme of the ionization chamber. Top view.

a1, a2, a3 and b1, b2, b3 are the input and output windows respectevely (beryllium, 3mm thick);
c1 is the window for scattered photons (beryllium, 5mm thick);
d is the stripped anode;
e is the projection of the outer dimensions of the cathode and the grid. The material of the IC body is stainless steel (20mm thick). The IC volume is 1.5 litre; $P \times V \simeq 150$ bar$\times$litre.

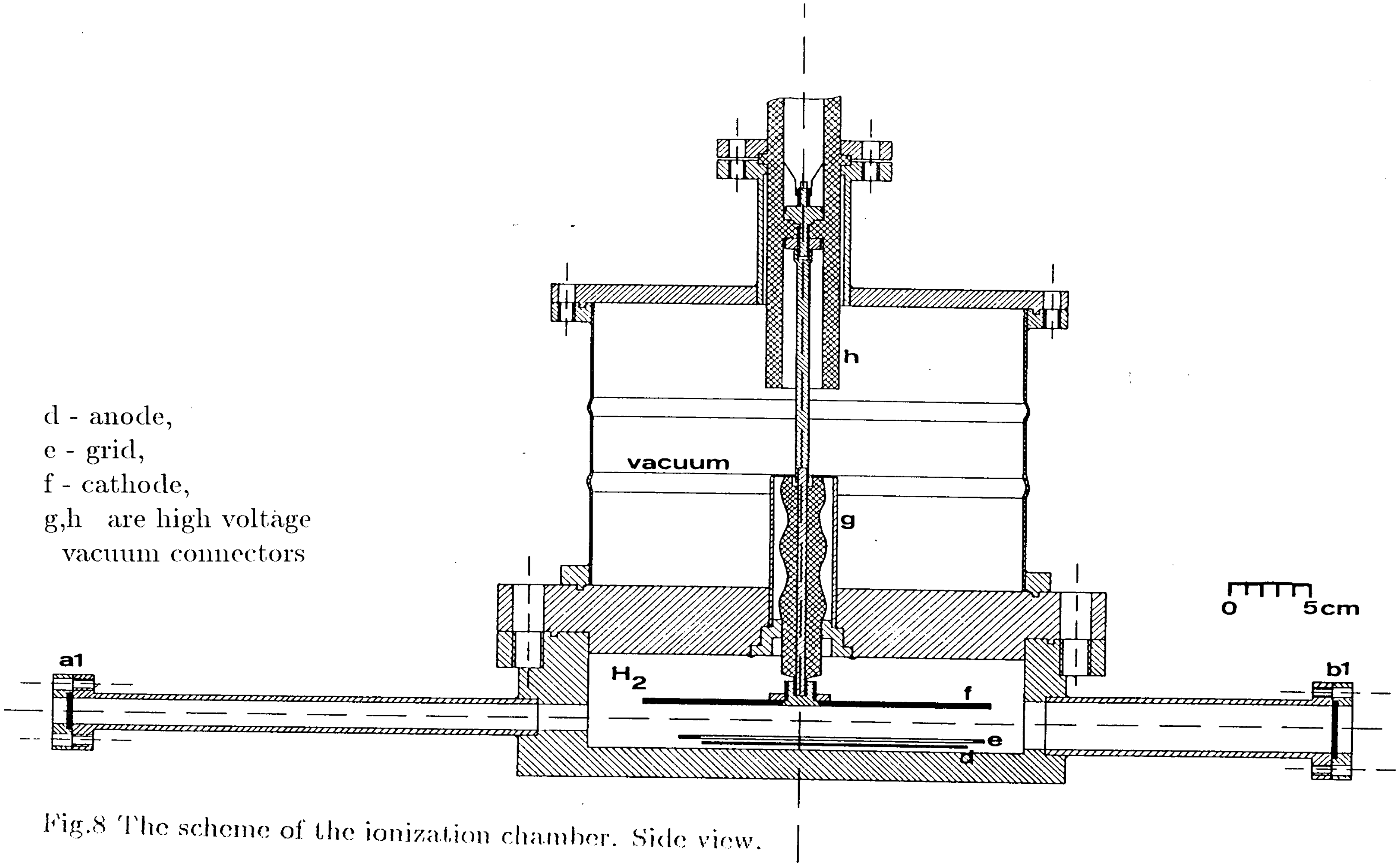

d - anode,
e - grid,
f - cathode,
g,h are high voltage vacuum connectors

Fig.8 The scheme of the ionization chamber. Side view.

The technology of the IC maintenance and detailed design will be described in the technical project separately.

IV. Electron-positron background; requirements to the electron beam.

The background anode current due to gas ionization by Compton electrons and e^+e^- - pairs was estimated assuming a continuous bremsstrahlung beam with the energy

$$W = \int_0^{E_0 \simeq 100MeV} [dN(\omega)/d\omega]\omega d\omega \simeq 4 \times 10^{12} MeV/s$$

passing through the 6cm long of the IC (sensitive volume), filled with hydrogen at 100bar pressure, $n_p = 3.24 \times 10^{22} p/cm^2$. Then in 450 hours of the beam time about 10^6 events at each scattering angle ($\theta_\gamma = 60^0$ and $\theta_\gamma = 135^0$) will be obtained. Here $dN(\omega)/d\omega$ is the energy spectrum formed after "filtration" of the incident bremsstrahlung produced in the target-radiator; E_0 is the maximum energy of the bremsstrahlung photons. The bremsstrahlung beam after the radiator passes through the 30cm polyethylene "filter" to attenuate the flux of low energy photons with $\omega \leq$ 1MeV. The lead collimators form a 1×2cm^2 beam on the IC. Charged particles produced by the photons on their way to the IC are deflected by magnetic field (Fig.2), so only the particles produced at a distance ≤10cm from the IC can reach it. The GEANT routine [15] has been used for estimation of the background. The interactions of the γ-quanta (Compton scattering, pair production) and of the secondary charged particles (bremsstrahlung, Moliere scattering, pair production, δ-electrons production, ionization loss) with materials has been taken into account. The energy deposition of the background electrons and positrons in the IC and the two-dimensional plot "energy deposition $vs.$ length of a track projection on the direction perpendicular to the plane of anodes" for detectable events have been calculated. Contributions of ionization by charged particles produced in the IC and outside have been calculated separately. These calculations were done for two orientations of anode strips at $\theta_p = 60^0$ and $\theta_p = 20^0$ (corresponding to scattering angles of photons $\theta_\gamma \simeq 60^0$ and $\theta_\gamma \simeq 135^0$). Most of the background ionization is contributed by the Compton electrons. The contribution of the pairs production is about 10%. The spectrum of the Compton electrons producing ionization in the IC is presented in Fig.9. The background anode current $i_b(t)$ is determined by the quantity of the charge arriving in the 0.5mm gap between the grid and the anode, accumulated within a track drift time of 2μs (the target with vertical dimension of 1cm). The values of $i_b(t)$ in the energy units of keV/100ns (100ns is the drift time of electrons from the grid to the anode) are given in Table I.

The electron current required for performance of the experiment during 450 hours has been estimated from the following assumptions:

1) the incident electron beam on a target-radiator of 0.1 rad.length (X_0) has the emitance of 4πmm$\times$mrad and has FWHM of 1mm. (Conditions satisfied, for example, by the electron Linac at Darmstadt);

2) the distance L between the target-radiator and the target-IC is (2-3)m; dimensions of the bremsstrahlung beam at the hydrogen target are 1×2 cm^2.

Bremsstrahlung energy on the IC-target, W, in units of the total bremsstrahlung energy produced by the radiator, W_0, is expressed

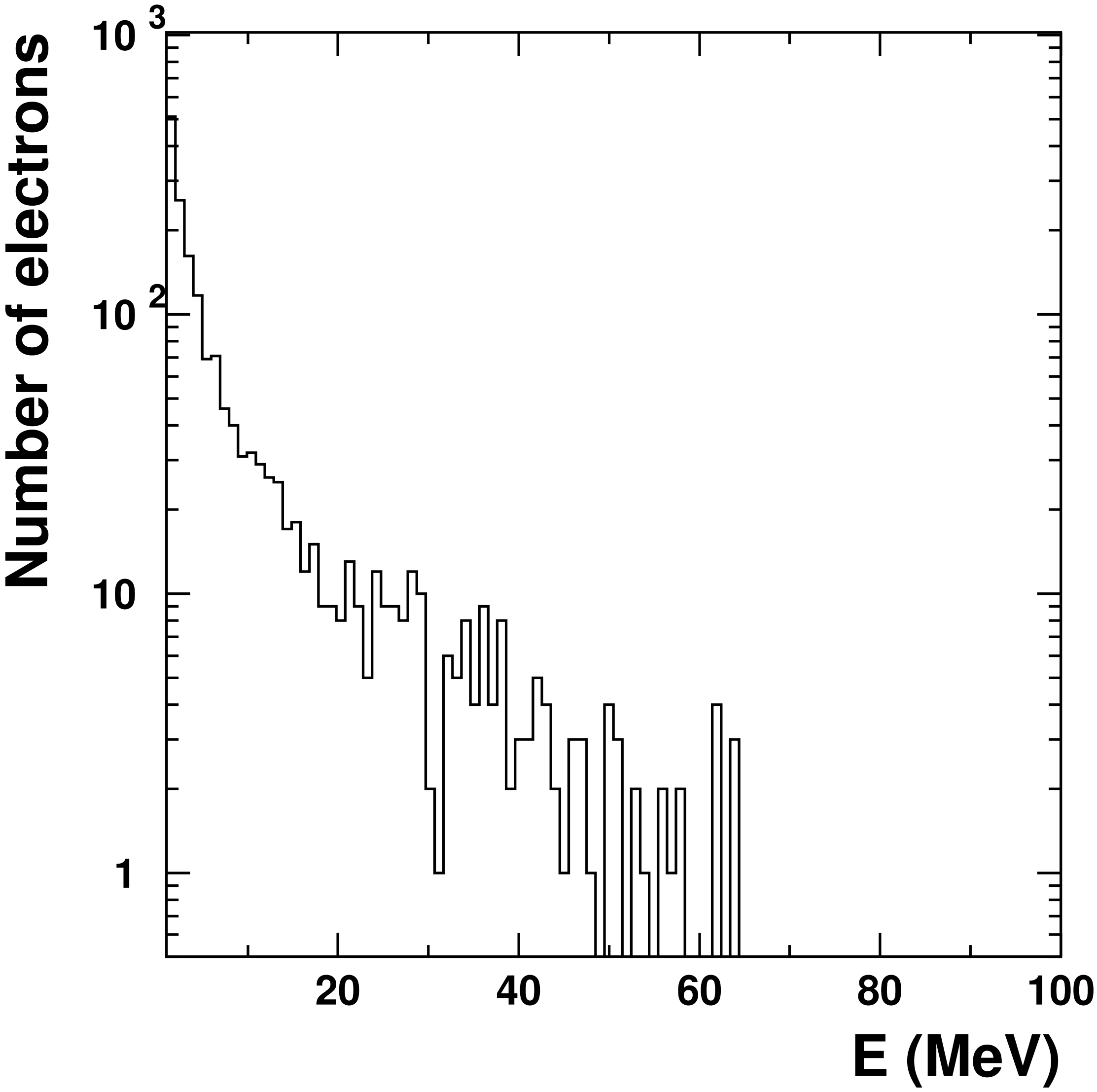

Fig.9 Spectrum of Compton electrons producing ionization in IC.

Table I

The average background current at the IC anodes in the units of keV/100ns. In brackets are the numbers of events during 100ns. (Thickness of H_2 between the IC and the end of the cleaning magnet is about 15cm.)

a - ionization due to photon scatterings inside the IC.

b - ionization by the particles produced upstream of the IC.

a+b - sum current (average and fluctuations).

N_a	$\theta_p = 60^0$			$\theta_p = 20^0$		
	a	b	a+b	a	b	a+b
1	14.5(2.2)	121.7(20.1)	136±28	38.8(4.2)	183.2(18.5)	223±47
2	16.5(2.8)	119.0(20.0)	135±28	38.8(4.2)	183.2(18.5)	229±53
3	21.8(3.7)	119.0(19.0)	141±30	62.0(5.3)	176.2(14.1)	238±54
4	27.4(4.4)	116.0(18.8)	143±30	82.0(6.9)	172.4(13.5)	254±52
5	29.9(5.2)	112.0(18.3)	142±29	106.0(8.5)	167.5(13.0)	274±59
6	36.4(6.1)	109.0(18.0)	145±30	116.0(9.8)	165.0(12.5)	281±58
7	41.5(6.7)	106.0(17.5)	148±30	135.0(11.0)	160.9(12.1)	296±62
8	45.1(7.3)	104.0(16.3)	149±31	147.0(12.0)	156.0(11.6)	303±62
9	49.8(8.0)	103.0(16.8)	153±31	157.0(13.2)	152.0(11.4)	309±62
10	55.7(8.6)	101.0(16.5)	157±31	177.5(17.8)	144.4(13.9)	327±58
11	56.7(9.4)	100.0(16.3)	157±31	188.0(15.6)	145.5(10.8)	334±65
12	58.7(10.1)	99.0(16.0)	158±31			
13	62.5(10.6)	99.0(16.0)	163±32			
14	66.1(11.1)	100.0(15.8)	166±32			
15	70.0(11.5)	96.5(15.5)	167±32			
16	69.2(11.6)	94.0(15.2)	163±32			
17	72.5(12.1)	92.6(14.9)	165±32			
18	79.6(12.4)	91.0(14.7)	171±32			
19	80.8(12.7)	90.0(14.4)	171±32			

as

$$k \equiv W/W_0 = 4 \cdot 10^{12}(MeV)/I(\mu A)\, 6.24 \cdot 10^{12}(t/X_0)E_0(MeV)$$

Here I is the current of the continuous electron beam, t is the radiator thickness, E_0=130MeV is the electron beam energy. The expression was estimated by Monte-Carlo simulation using the formula from [16] for bremsstrahlung angular distribution, taking into account Moliere scattering. As a result we have:

$$k = 0.02,\ \ I = 3.1\mu A\,(L = 2m)\,;$$

$$k = 0.014,\ \ I = 4.4\mu A\,(L = 3m)\,.$$

However, taking into account absorption of the bremsstrahlung quanta in the polyethylene filter (30cm thick), we need to increase the current by a factor of two:

$$I = 6.2\mu A\,(L = 2m)\,;\ \ I = 8.8\mu A\,(L = 3m)\ .$$

V. Neutron background.

This background arises from the elastic scattering of neutrons on hydrogen in the IC volume, produced by photonuclear reactions Pb(γ,n) in collimator, C(γ,n) in polyethylene filter and Be(γ,n) in the input window of the IC.

The background estimation was done under certain reasonable assumptions and with available experimental data. We assumed that all the incident bremsstrahlung energy, W_0, is absorbed in the part of Pb collimator placed at R=1.5m distance from the IC. The number of the incident γ-rays, N($\overline{\omega}_i$), producing neutrons in Pb(γ,xn)-reactions is given by

$$N(\overline{\omega}_i)\ \simeq\ \frac{\sigma_{Pb(\gamma,xn)}(\overline{\omega}_i)}{\sigma_{Pb(Compt)}(\overline{\omega}_i) + \sigma_{Pb(pair)}(\overline{\omega}_i)} N_0(\overline{\omega}_i) \equiv A(\overline{\omega}_i)N_0(\overline{\omega}_i)\ \ ,$$

where $\sigma_{Pb(\gamma,xn)}(\overline{\omega}_i)$ is the known total cross section of Pb(γ,xn)-reaction [17,18] with emission of one or several neutrons. The intensity of these events is

$$B \simeq \frac{W_0}{E_0}\int_{(\gamma,1n)threshold}^{E_0\simeq 100MeV}\frac{A(\overline{\omega}_i)}{\omega_i}d\omega_i \approx 2.5\times 10^{10}s^{-1}$$

for I$\simeq$3μA, and taking into account the multiplicity x of photoneutrons, the intensity of neutrons is estimated N$\simeq$3.6$\times 10^{10}$ s^{-1}. In the range $\Delta_1\omega$ of photon energies from $(\gamma,1n)$ threshold up to 30MeV we have $N_1 \simeq 2.8\times 10^{10}$ neutrons/s, while in the interval $\Delta_2\omega$ of (30–100)MeV there are $N_2 \approx 0.8\times 10^{10}$ neutrons/s. The neutron angle distribution is assumed to be isotropic and hence $N' = S/(4\pi R^2)N$ neutrons/s will pass through the volume of the IC after Pb collimator and polyethylene filter. For the IC cross-section S$\approx$10cm^2 $N_1' \approx 10^6$ 1/s and $N_2' \approx 2.8\times 10^5$ 1/s.

The energy spectrum photoneutrons [19,20] produced by γ-rays in the energy range $\Delta_1\omega$ has a maximum at $E_{n(0)} \simeq$ 2MeV, which is described by statistical model with the exception of high energy part of the spectrum above 5MeV. However this part of the neutron spectrum does not exceed (10–20)%. After moderation in polyethylene the energy of neutrons does not exceed 200keV. Therefore recoil protons in the IC, produced in (n,p) elastic scattering, will have low energies compared to Compton scattered protons and can be easily discriminated. The elastic (n,p)-scattering cross sections was taken from [21].

We do not have a spectrum of photoneutrons producted by γ-rays in the energy interval $\Delta_2\omega$ ($\approx$40-100MeV) for quantitative estimation of corresponding background. However apparently we will overestimate the background assuming that most of these photoneutrons have no time for slowing down to low enough energies and are able to create the background recoil protons with energy comparable to that of useful recoil protons. Then, assuming $\overline{E}_n \approx$5MeV, the result of background estimation is 1.5×10^4 p_{recoil}/s in the IC volume, i.e. 3×10^{-2} $p_{recoil}/200\mu$s. Taking into account the rejection of background events by selection of the events which are compatible with kinematics of the reaction $\gamma + p \to \gamma' + p'$, we infer that background level is acceptable.

Estimation of background due to C(γ,xn) reaction in polyethylen filter and Be(γ,xn) reaction [22-24] in the inlet window of the IC shows several times lower level compared to Pb(γ,xn) reaction. The filter and the window are placed at 1m and 30cm from IC, respectively.

The NaI(Tl) crystal should be surrounded by an anticoincidence plastic shielding scintillator in order to identify and reject both charged particles coming from cosmic rays and electrons and positrons emerging from the target. A heavy shielding by lead, concrete and polyethylen is proposed also to absorb the photons and neutrons scattered by collimators. Some previous experiments (for example [8]) suggest that the count of background photons detected by NaI(Tl)-spectrometer will not exceed essentialy the number of useful events.

VI. Estimation of systematic errors in measurement of $\mathbf{d}\sigma(\overline{\omega}_i, \overline{\theta})/\mathbf{d}\Omega$.

The use of formulae (7) and (8) for evaluation of differential cross-sections involves some systematic biases, which we are going to consider now.

1) It is necessary to provide constant efficiency of detection of the recoil protons in the energy range 0.4-8MeV. This is achieved by selection of scattering events taking place in a definite effective

volume of the IC. We arrange the anode strips in such a way that a track of a recoiled proton, arising over a given strip, cannot penetrate into the volume of the preceeding strip (Fig.10), $\theta_{strip} \simeq \theta_p + |\Delta\theta_p|_{max}$, where $|\Delta\theta_p|_{max} \simeq 5^0$ is the provisional angle shift of the strip system, compensating the finite inlet aperture of the IC. We reject all the scattering events with any signals on the first anode (this eliminates all scatterings in the gas inside the IC vessel but before the anode system), and also the events with single signals on the last anode, not accompanied by time-coincident signals on the preceeding anode. The signals on the last anode are rejected to eliminate the scattering events with protons leaving the sensitive volume and with their energy not measured. So we obtain only the events of scattering in the effective volume over all the anodes except the first and the last ones.

2) Non-negligible threshold value can lead to some miscounting. For example, a scattering event can take place over the 1-st anode near its rear edge, so that the fraction of the proton track over the 1-st anode is too small to provide the signal above the threshold. Such an event will be acquired, though it should be rejected. Let us estimate the number of such events.

   The gas thickness, where the energy deposition of a long-range proton is less than the energy threshold ($\Delta E \sim$ 300keV for the typical 100ns pulses), does not exceed $\Delta R \sim 3mm$ (Fig.10). With the angle between the track and the strip $\sim 5^0$ we have the width of the non-effective edge of the strip $h \sim \Delta R sin 5^0$, and this makes less than 0.1% of the total length of the IC.

   These "excessive" events, counted due to unefficiency of the 1-st anode, are compensated by the missing events of scattering on the last-but-one anode, which had deposited too low energy on it

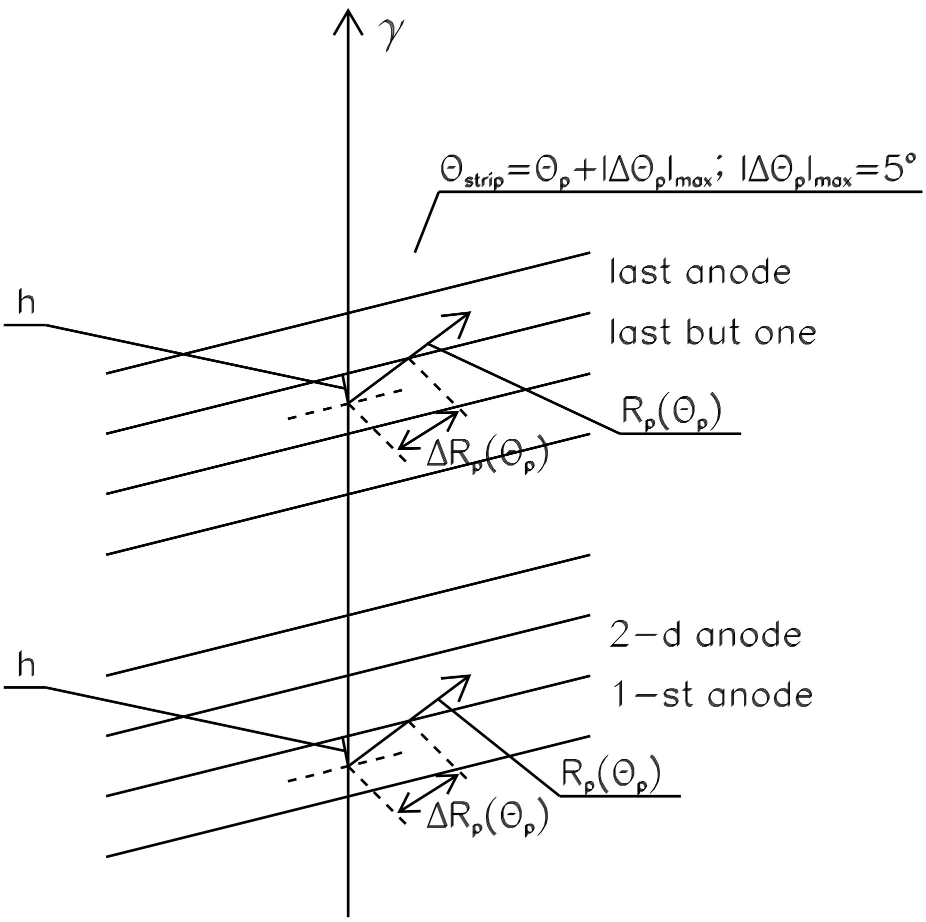

Fig.10 Illustration to definition of effective volume IC.

and were rejected. With equal thresholds and uniform beam these corrections cancel each other.

We have used the expressions (7,8) assuming that the scattered photons with different energies ω_i' have the same effective solid angle $\Delta\Omega(\omega_i)$. In reality it is determined by incomplete absorption of γ-quanta in the lead collimator and obviously depends on ω_i'. We have calculated the energy dependence of the photon attenuation and the ratio $\Delta\Omega(\omega_i)/\Delta\Omega(geom.)$, for two lead collimators 60cm long with rectangular holes of $2 \times 6cm^2$ and $10 \times 10cm^2$ (Fig.11). One can see that the effective solid angles for ω_i = 15MeV and ω_i' =100MeV differ only by $(1.3 \pm 0.05)\%$. For the second collimator, used in the γe-scattering, the relative change in the solid angle is negligible (Fig.12).

3) The requirements to the energy scale accuracy of γ-spectrometer (ω') and also to mounting of the scattering angles ($\theta_{\gamma e}; \theta_{\gamma p}$) are illustrated at Fig.13-15, where we show the energy dependencies of relative change of the differential cross section on variations of the energy ω', $\delta\omega'/\omega' = 10^{-2}$ for $\theta_{\gamma p} = 60^0$, 135^0 (for two values of $\overline{\alpha} = 14$ and $\overline{\alpha} = 6$), $\theta_{\gamma e} = 1.98^0$ (Fig.13) and also due to $\theta_{\gamma e}$ change of 0.01^0 (for $\theta_{\gamma e} = 1.98^0$; Fig.14) and $\theta_{\gamma p}$ change of 1^0 (for $\theta_{\gamma p} = 60^0$, 135^0 and $\overline{\alpha} = 9$ and 15; Fig.15). The scattering angle $\theta_{\gamma e}$ can be established with required accuracy by forming the bremsstrahlung source of 1mm diameter and using the string target with $\sim 0.1mm$ diameter, 3-4m distant from bremsstrahlung source, and with the detector of scattered photons at 10-20m from the target. The direction of incident bremsstrahlung is determined with uncertainty $\leq 0.01^0$. The angle between this direction and the scattered photons detected by the γ-spectrometer is determined with uncertainty of $\leq 0.006^0$ (if

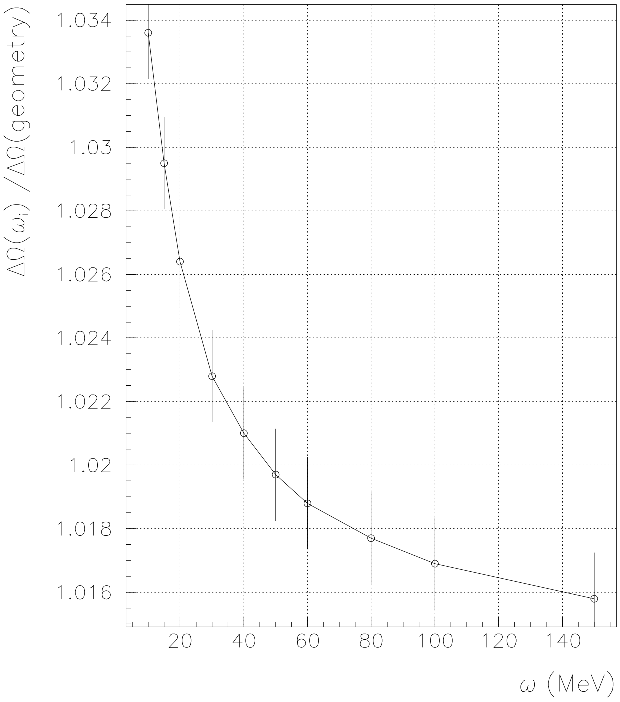

Fig.11 Energy dependence of solid angle for detection of the photons scattered by protons (collimator $2{\times}6\,cm^2$).

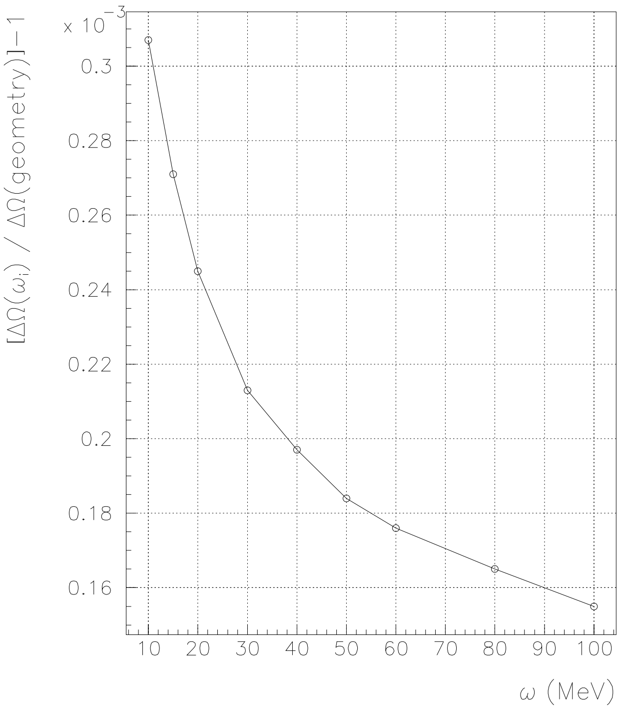

Fig.12 The same as in Fig.11 for detection of the photons scattered by electrons (collimator $10{\times}10\,cm^2$).

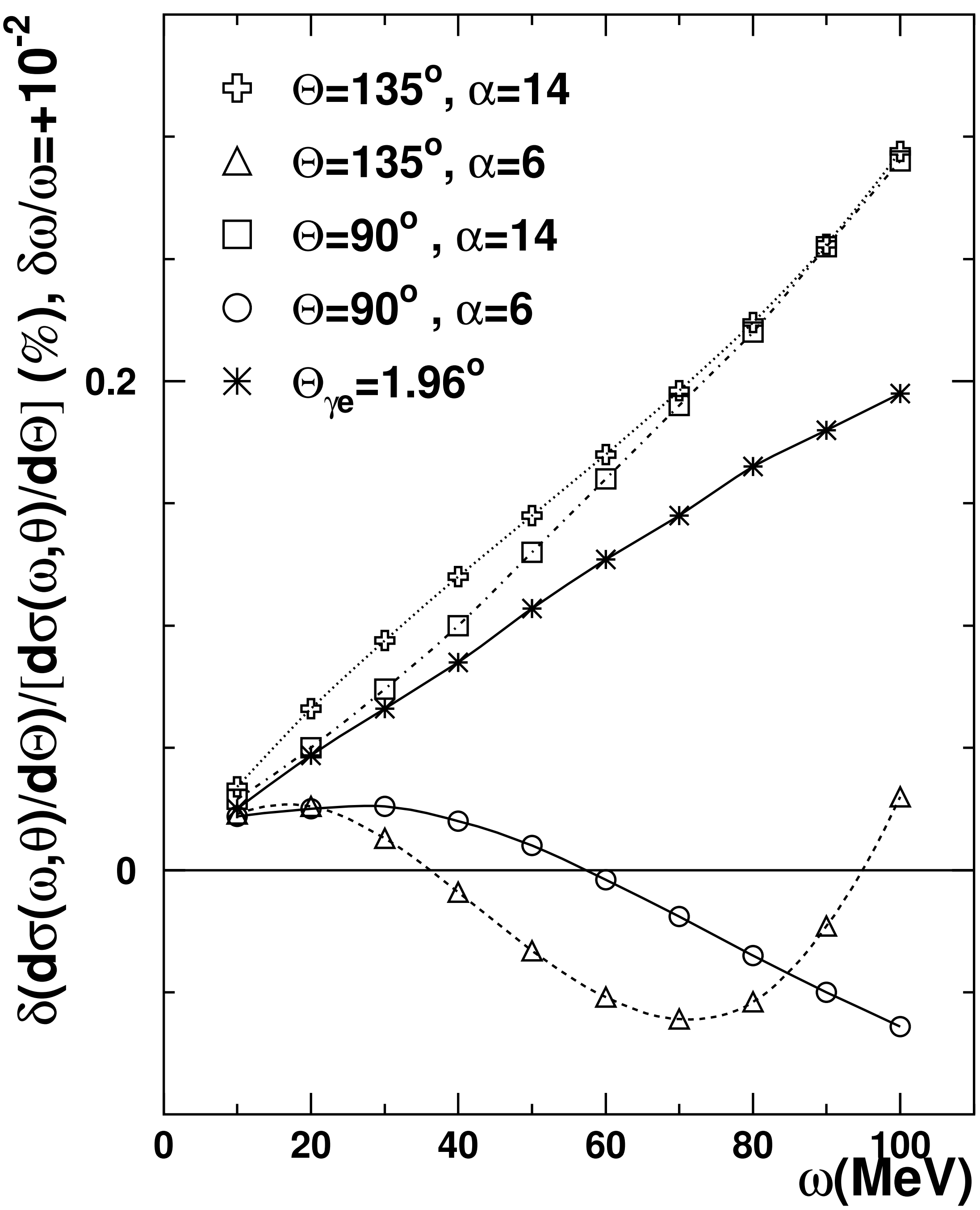

Fig.13 Energy dependence of the relative differential cross sections changes due to change of ω' on value $\delta\omega'/\omega' = 10^{-2}$ for θ of 90^0 and 135^0 (if $\overline{\alpha}$ are of 14 and 6) and $\theta_{\gamma e}$ of 1.98^0.

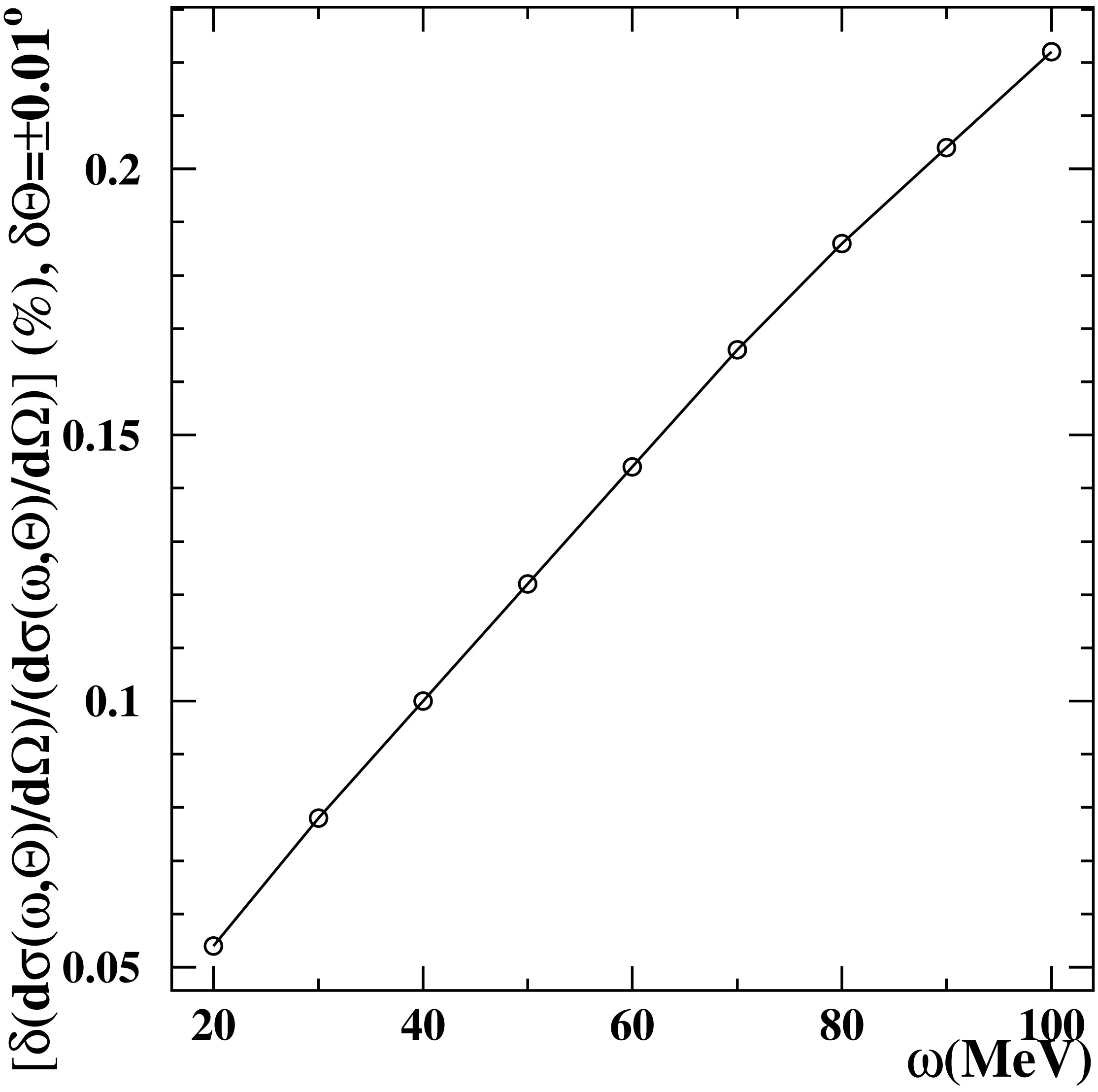

Fig.14 Relative change of γe-scattering differential cross section by change of a scattering angle $\theta_{\gamma e} = 1.98^0$ on value of 0.01^0 for different values ω.

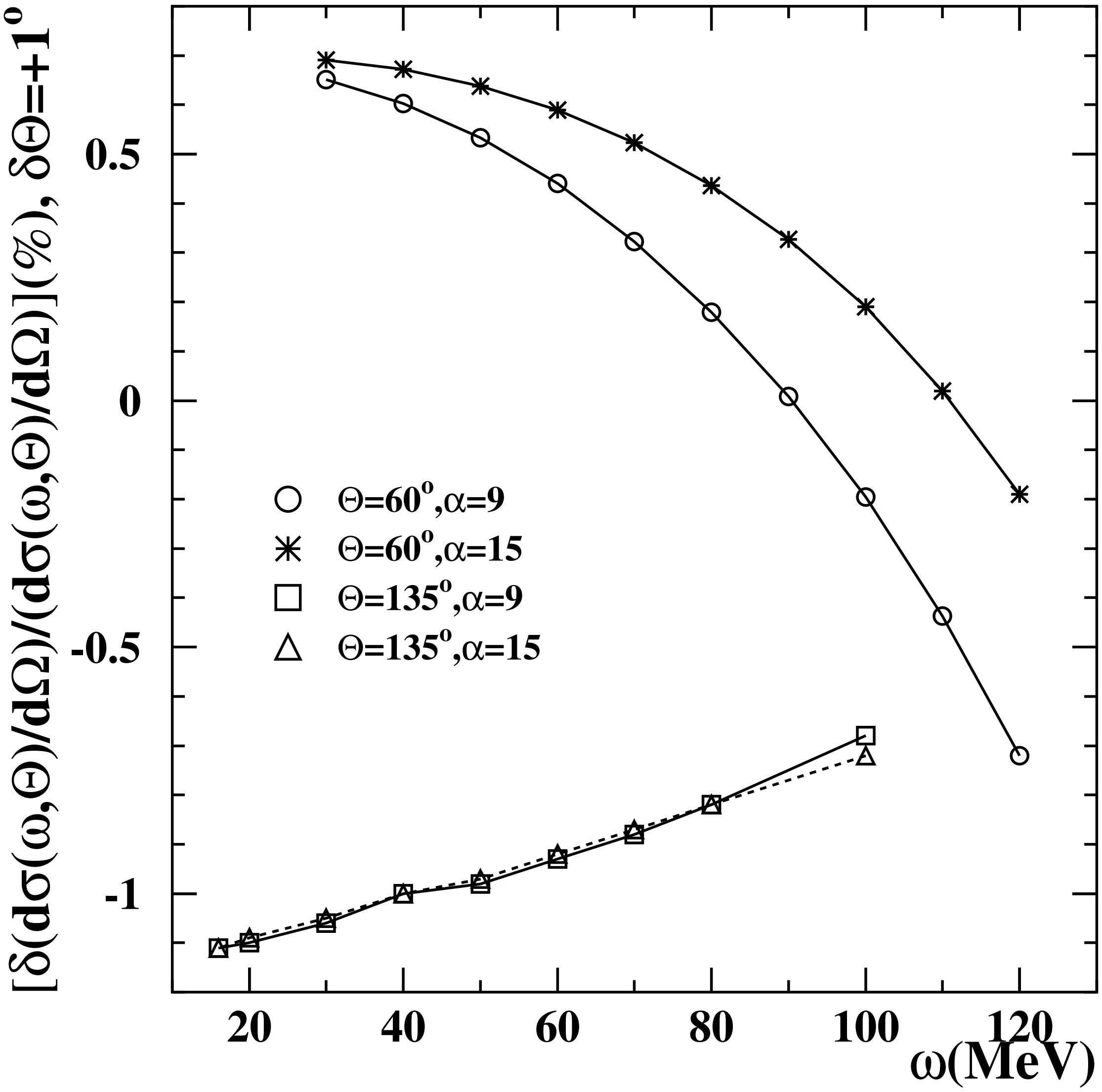

Fig.15 Energy dependence of γp-scattering differential cross sections by change of a scattering angle on value of $\delta\theta = \pm 1^0$.

the lengths of $\sim 100mm$ and $\sim 10000mm$ are measured with precision $\pm 1mm$ and $\pm 10mm$, respectively). [Note that the counting rate of the useful events of (γe)-scattering measurements by means of a string target (for example, an Al string of 0.3mm diameter) is $\sim$ 100 1/s; the beam time required for this experiment is few hours.]

4) The expression (7) does not take into account the absorption of scattered photons on their way to the NaI-spectrometer. The attenuation coefficients of photons for 5mm thick Be output window of the IC and 60cm of the air and also 10m of the air in case of γe-scattering measurements are $\approx$0.99 and $\approx$0.98, respectively. The energy dependence of these coefficients is small, thus differ only by 1% for 15MeV and 100MeV quanta. Hence the uncertainty of the ratio $\sigma_i^e(100)/\sigma_i^e(15)$ due to this absorption will not exceed 0.05%.

5) We suppose to use a spectrometer similar to one of two existing high resolution NaI(Tl) total absorption scintillation counters. One is in Brookhaven [25], a 25cm diameter $\times$ 35cm long NaI single-element detector with 2.2% FWHM resolution at 22MeV. The second is in Boston University [26], 50cm diameter $\times$ 55cm long NaI multi-element detector with 1.3% FWHM resolution at 130MeV. Typical response functions of NaI-spectrometers obtained by Monte Carlo simulation of the experiment are shown in Fig.16,17 (of Brookhaven type) and Fig.18,19 (of Boston type) for radiation entrance windows of 2.5$\times$2.5cm^2 and 10$\times$10cm^2 (a - ω =15MeV, b - ω =100MeV). As one can see, the Brookhaven type NaI spectrometer must have identical radiation entrance windows for both (γ,p)- and for (γ,e)-scattering in order to ensure the same response functions. With Boston type NaI the same response functions can be obtained with different for radiation entrance win-

dows.

Thus we come to conclusion that it is possible to make the total systematic error of the differential cross sections $d\sigma(\overline{\omega}_i, \overline{\theta})/d\Omega$, obtained from the analysis of experimental data with the expression (5), less than 1%.

Acknowledgements.

The authors thank A.Lvov, V.Petrunkin (Lebedev Institute, Moscow), A.Nathan (University of Illinois, Urbana), G.Ganzha, A.Krivshich, G.Petrov, G.Schklyarevsky and V.Trofimov (PNPI, Gatchina) for useful discussions.

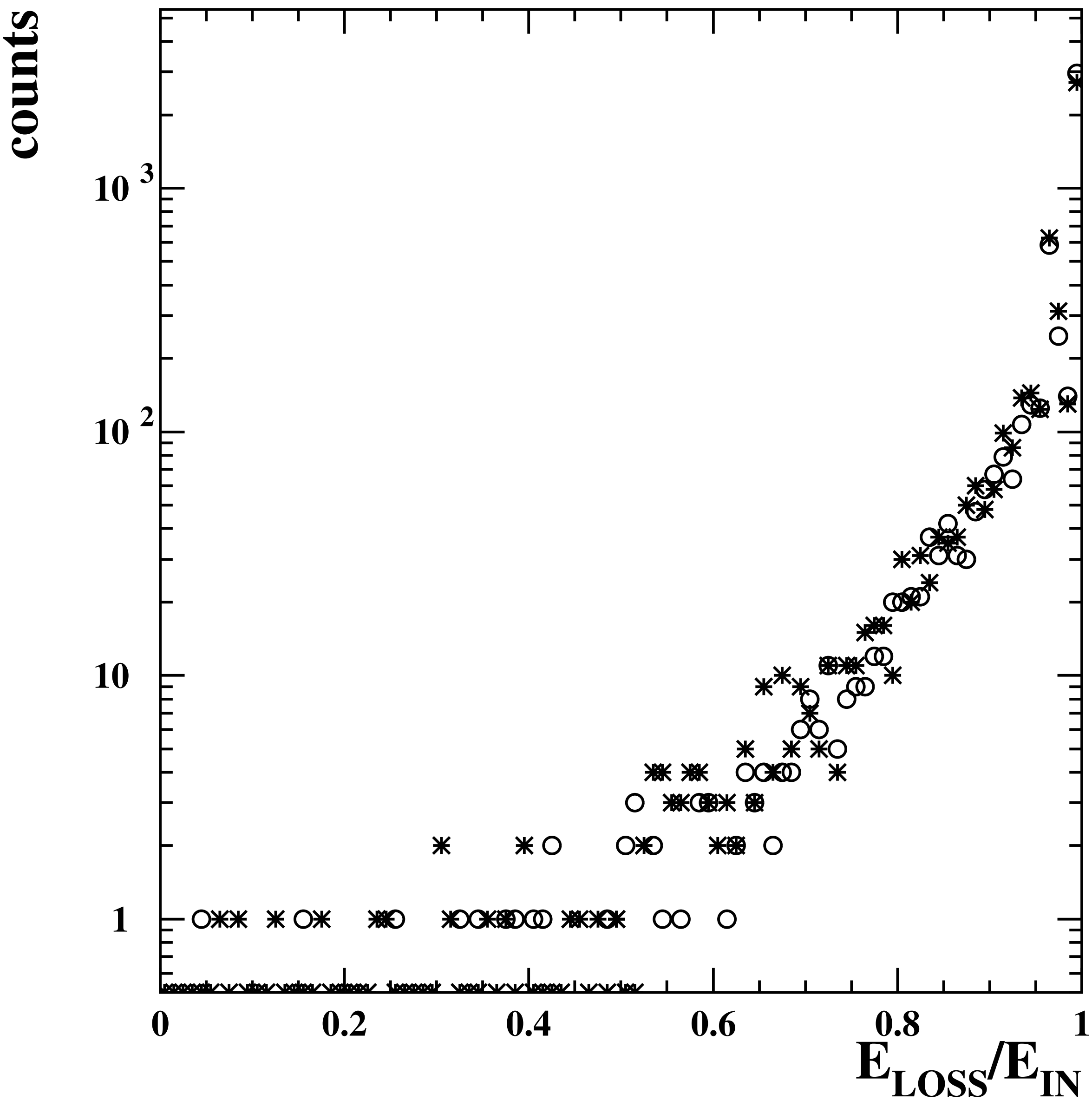

Fig.16 Response functions of the NaI-spectrometer (Brookhaven type NaI [25]) for radiation entrance windows with dimensions of $2.5{\times}2.5\text{cm}^2$ ($\star$) and $10{\times}10\text{cm}^2$ ($\circ$); ω=15MeV.

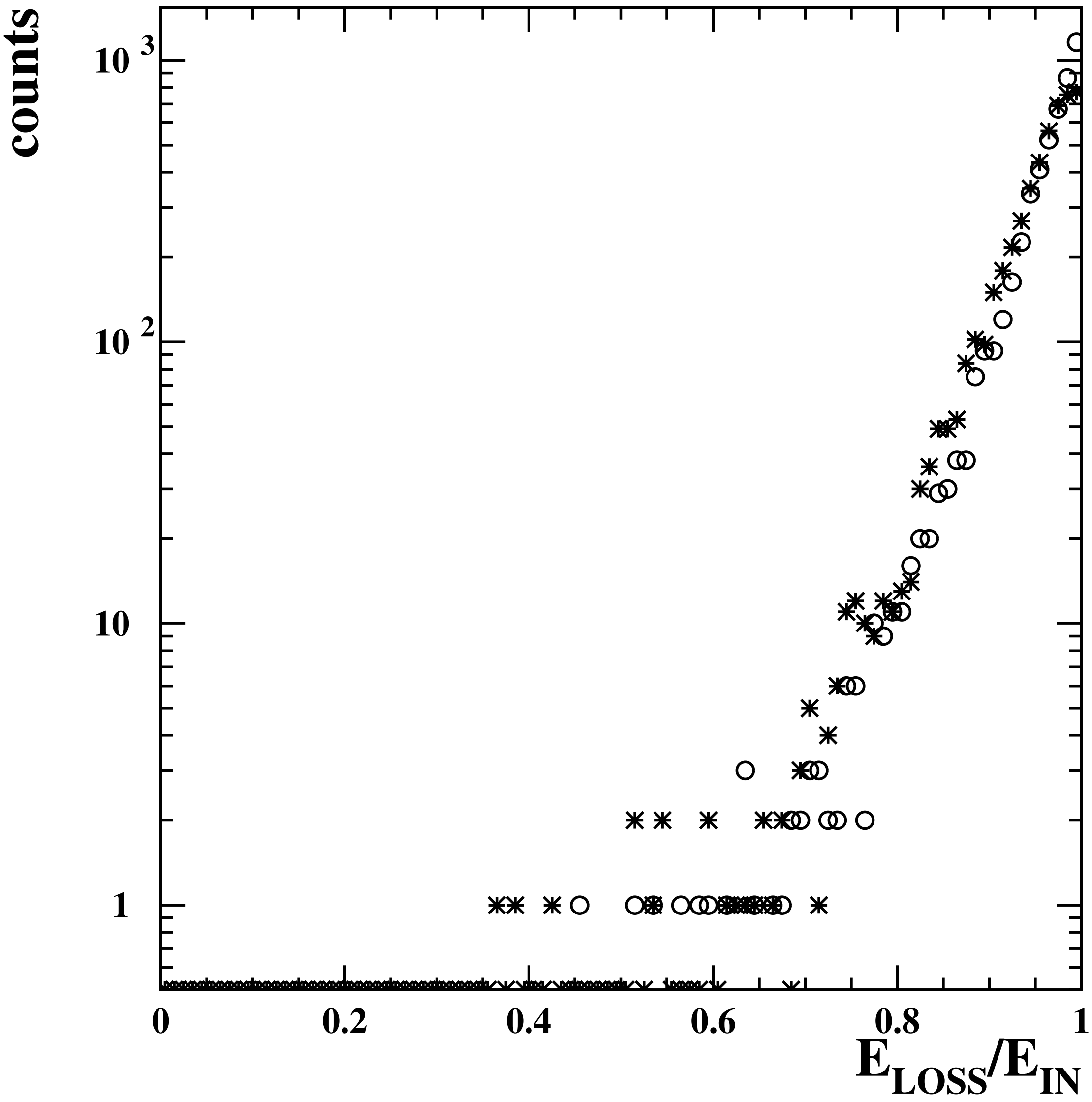

Fig.17 The same as Fig.16 for ω=100MeV.

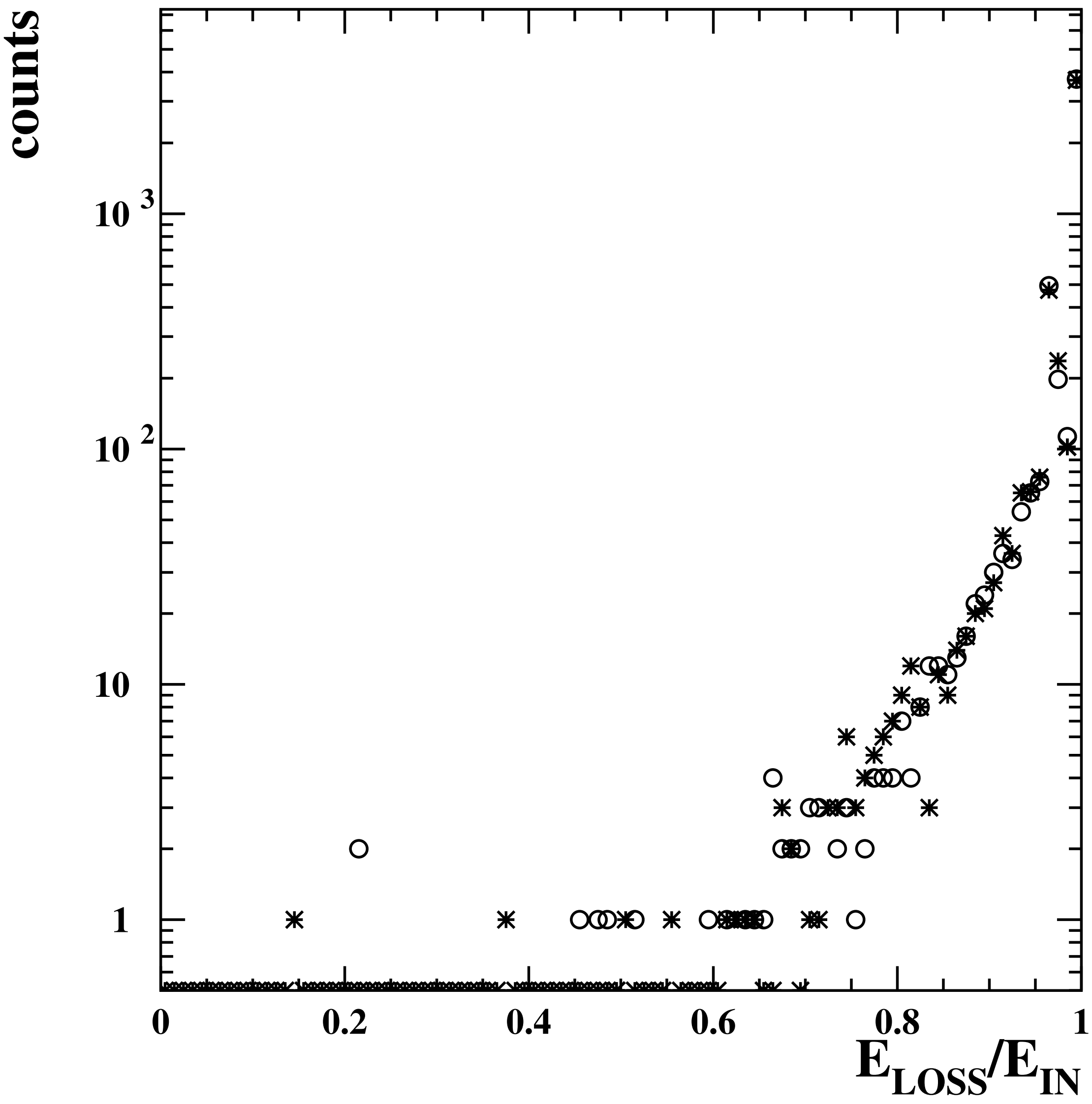

Fig.18 The same as Fig.16 for Boston type NaI [26].

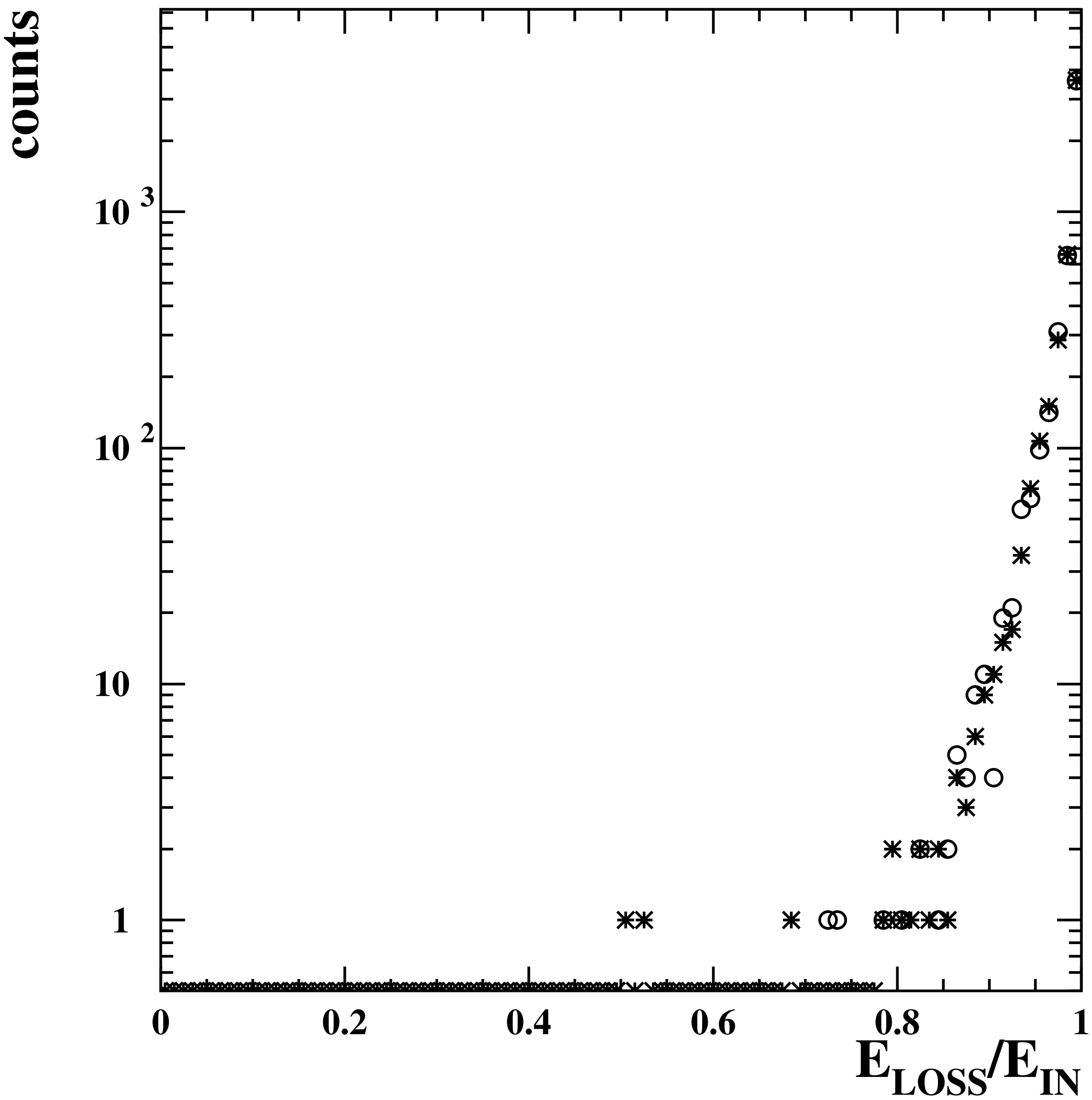

Fig.19 The same as Fig.17 for Boston type NaI [26].

References

1. *Petrunkin V.A.* //Fiz. Elem. Chastits At. Yadra, 1981 V.12 P.692 [Sov. J. Part. Nucl., 1981 V.12 P278.]
2. *Lvov A.I., Petrunkin V.A.*, Lebedev inst. preprint No.258 P.1988.
3. *Lvov A.I., Petrunkin V.A.* //JETP Lett., 1983 V.37 P.63.
4. *Powel J.L.* //Phys. Rev., 1949 V.75 P.32.
5. *Gell-Mann M., Goldberg M.L., Thirring W.E.* //Phys. Rev., 1954 V.95 P.1612.
   Baldwin A.M. //Nucl. Phys., 1960 V.18 P.1612.
   Damashek A.M. Gilman F.J. //Phys. Rev., 1970 V.D1 P.1319.
6. *FederspielF. J. et al.* //Phys. Rev. Lett., 1991 V.67 P.1511.
7. *Lvov A.I.* //Yad. Fiz., 1981 V.34 P.1075. [Sov. J. Nucl. Phys., 1981 V.34 P.597].
8. *Baranov P.S. et al.* //Yad. Fiz., 1975 V.21 P.689 [Sov. //J. Nucl. Phys., 1975 V.21 P.355].
9. *Petrunkin V.A., Lvov A.I.* Proc. 8-th Intern. Seminar on Electromagnetic Interactions of Nuclei at Low and Medium Energy, Moscow December 1991, Nauka Moscow 1992.
10. *Zieger A. et al.* //Phys. Lett., 1992 V.B278 P.34.
11. *Hallinat E.L. et al.* //Phys. Rev., 1993 V.C48 P.1497.
12. *Lvov A.I.* (private communication).
13. *Balin D.V. et al.* Preprint LNPI-964, 1984.
14. *Balin D.V. et al.* Preprint LNPI-1630, 1990; *Balin D.V. et al.* Muon Cat. Fusion, ,1990/91 V.5/6 P.481;
    Balin D.V. et al. Muon Cat. Fusion ,1992) V.7 P.1.
15. *Brun R. et al.* GEANT3. CERN report DD/EE/84-1, September 1987.

16. *Lanzl L.H., Hanson A.O.* //Phys. Rev., 1951 V.83 P.959.

17. *Veyssiere A. et al.* //Nucl. Phys., 1970 V.A159 P.561.

18. *Lepzetre A. et al.* //Nucl. Phys., 1981 V.A367 P.237.

19. *Lazareva L.E. et al.* //Yad. Fiz., 1974 V.20 P.242.

20. *Mc Neil K.G. et al.* //Can. J. Phys., 1970 V.48 P.950.

21. *Vlasov N.A.* The neutrons Nauka, Moscow, 1971 P.197.

22. *Ahrens J. et al.* Intern. Conf. on Photonucl. Reactions and Applications, Asilomar, Proceedings, 1973 V.1 P.23.

23. *Ahrens J. et al.* //Nucl. Phys. 1975 V.A251 P.479.

24. *Berman B.L.* Atomic Data and Nuclear Data Tables, 1975 V.15 P.319-390.

25. *Sandorfi A.M. and Collins M.T.* //Nucl. Instr. & Methods in Phys. Research, 1984 V.222 P.479.

26. *Miller J.P. et al.* //Nucl. Instr. and Methods in Phys. Research, 1988 V.A270 P.431.

Appendix

This appendix contains the results of calculations of differential cross section $d\sigma(\omega,\omega',\theta)/d\Omega$ of inelastic photon scattering with pair production at Z=1 coulomb center, in the lower order of perturbation theory. The six diagrams of processes taken into account are shown on the Fig.1A[1]. The cross-section for photon scattering angles of θ=60, 90, and 140^0, integrated over momenta of electron and positron, are in the table IA. The energies of incident and scattered photons, ω and ω', are given in MeV, and the cross-sections - in $cm^2/MeV\ \ ster \times 10^{34}$. The ratio of the yield of inelastic scattered photons, $Y_{\gamma(\gamma',e^+e^-)}(\omega',\theta)$, to the yield of elastic scattered photons, $Y_{\gamma,p}(\omega',\theta)$, both integrated over the spectrum of incident bremsstrahlung with $E_{\gamma max} = 130$MeV, is shown on the Fig.2A.

In the table IIA are shown the energy intervals of protons, $(E_p^{max} - E_p^{min})$, recoiled in inelastic scattering to $\theta = 60^0$ with pair production, when the incoming photon has the energy ω, and the scattered photon - ω'. Also the energies of recoil protons E_p^{Compt} from the elastic scattering are presented.

[1] We thank G.M.Shklarevsky for these calculations and for permission to use these results prior to publication.

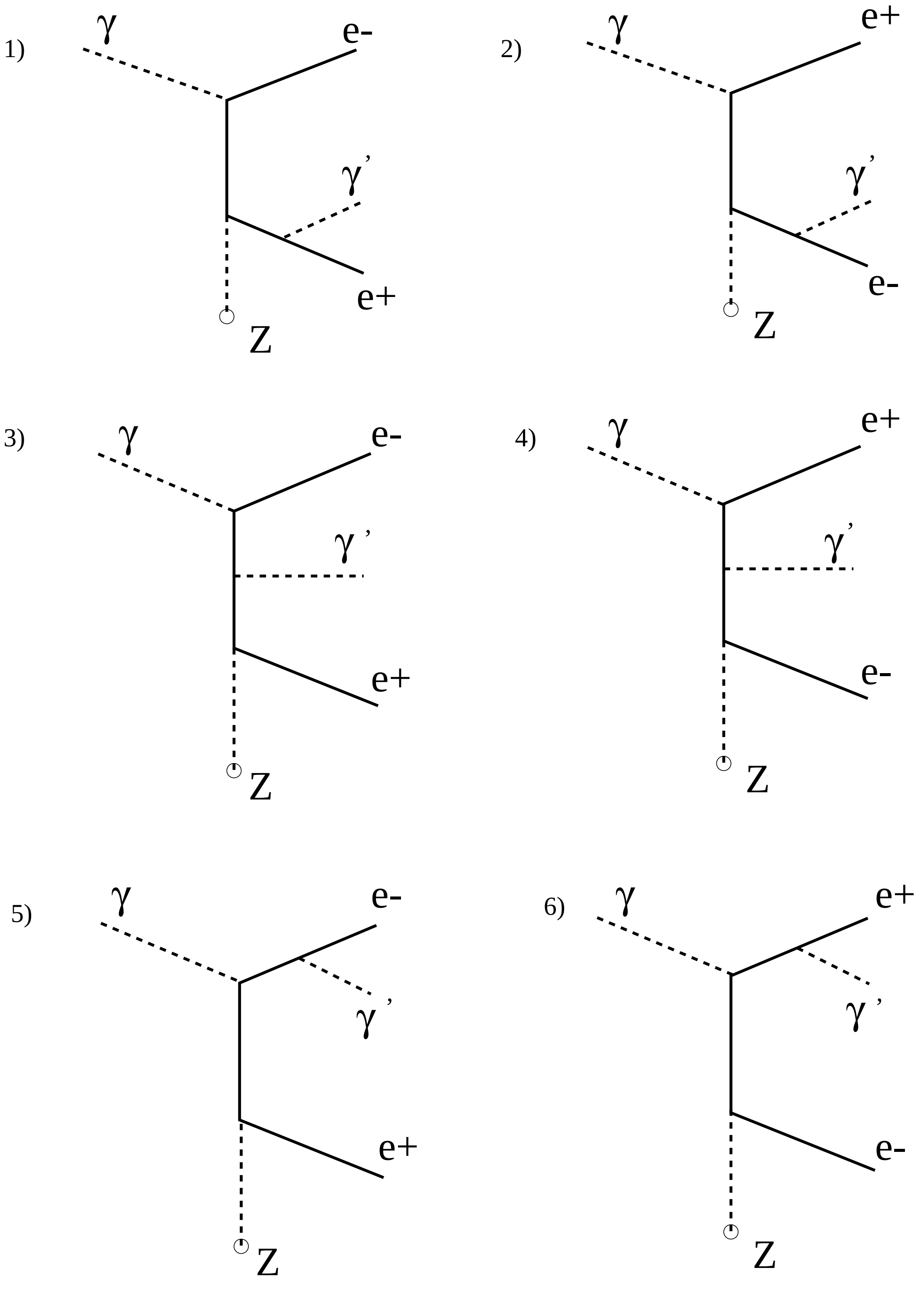

Fig.1A Six diagrams of $\gamma + p \rightarrow \gamma' + e^+e^- + p'$ processes taken into account.

Table IA

Differential cross section of the inelastic gamma-proton scattering with e^+e^--pair production, $d\sigma(\omega, \omega', \theta)/d\omega' d\Omega \times 10^{34} (cm^2/MeV \cdot sr)$.

ω-incident photon energy (MeV)
ω'-scattered photon energy (MeV)
θ-scattering angle

$$\theta = 60^0$$

ω' / ω	29.	39.	49.	59.	69.	79.	89.	99.	109.
35.	6.828	0.000	0.000	0.000	0.000	0.000	0.000	0.000	0.000
40.	5.892	3.932	0.000	0.000	0.000	0.000	0.000	0.000	0.000
45.	5.144	3.474	0.000	0.000	0.000	0.000	0.000	0.000	0.000
50.	4.538	3.094	2.248	0.000	0.000	0.000	0.000	0.000	0.000
55.	4.039	2.774	2.033	0.000	0.000	0.000	0.000	0.000	0.000
60.	3.623	2.504	1.847	1.418	0.000	0.000	0.000	0.000	0.000
65.	3.274	2.274	1.686	1.303	0.000	0.000	0.000	0.000	0.000
70.	2.976	2.076	1.547	1.201	0.958	0.000	0.000	0.000	0.000
75.	2.720	1.905	1.424	1.110	0.890	0.000	0.000	0.000	0.000
80.	2.498	1.755	1.317	1.030	0.829	0.681	0.000	0.000	0.000
85.	2.304	1.624	1.222	0.959	0.774	0.638	0.000	0.000	0.000
90.	2.134	1.507	1.138	0.895	0.725	0.599	0.504	0.000	0.000
95.	1.983	1.404	1.062	0.838	0.680	0.564	0.475	0.000	0.000
100.	1.849	1.312	0.995	0.786	0.640	0.532	0.449	0.384	0.000
105.	1.729	1.229	0.934	0.740	0.603	0.502	0.425	0.364	0.000
110.	1.662	1.155	0.879	0.697	0.570	0.475	0.403	0.346	0.300
115.	1.525	1.088	0.829	0.659	0.539	0.450	0.383	0.329	0.286
120.	1.437	1.026	0.783	0.623	0.511	0.428	0.364	0.313	0.273
125.	1.357	0.971	0.742	0.591	0.48	0.407	0.346	0.299	0.261

$\theta = 90^0$

ω' / ω	19.	29.	39.	49.	59.	69.	79.	89.	99.
25.	3.079	0.000	0.000	0.000	0.000	0.000	0.000	0.000	0.000
30.	2.678	1.247	0.000	0.000	0.000	0.000	0.000	0.000	0.000
35.	2.330	1.156	0.000	0.000	0.000	0.000	0.000	0.000	0.000
40.	2.040	1.056	0.599	0.000	0.000	0.000	0.000	0.000	0.000
45.	1.801	0.959	0.567	0.000	0.000	0.000	0.000	0.000	0.000
50.	1.602	0.872	0.531	0.338	0.000	0.000	0.000	0.000	0.000
55.	1.435	0.795	0.494	0.324	0.000	0.000	0.000	0.000	0.000
60.	1.295	0.727	0.460	0.307	0.211	0.000	0.000	0.000	0.000
65.	1.175	0.667	0.427	0.291	0.204	0.000	0.000	0.000	0.000
70.	1.072	0.615	0.398	0.274	0.195	0.142	0.000	0.000	0.000
75.	0.983	0.568	0.371	0.259	0.187	0.137	0.000	0.000	0.000
80.	0.906	0.527	0.347	0.244	0.178	0.133	0.100	0.000	0.000
85.	0.838	0.491	0.325	0.230	0.169	0.128	0.098	0.000	0.000
90.	0.778	0.458	0.305	0.217	0.161	0.123	0.095	0.074	0.000
95.	0.724	0.428	0.287	0.206	0.153	0.118	0.091	0.072	0.000
100.	0.677	0.402	0.271	0.195	0.146	0.113	0.088	0.070	0.056
105.	0.634	0.378	0.256	0.185	0.139	0.108	0.085	0.068	0.055
110.	0.595	0.356	0.242	0.176	0.133	0.103	0.082	0.066	0.053
115.	0.560	0.336	0.229	0.167	0.127	0.099	0.079	0.064	0.052
120.	0.529	0.318	0.217	0.159	0.121	0.095	0.076	0.062	0.051
125.	0.500	0.302	0.207	0.152	0.116	0.091	0.073	0.060	0.049

$\theta = 140^0$

ω' / ω	14.	24.	34.	44.	54.	64.	74.	84.	94.
20.	1.053	0.000	0.000	0.000	0.000	0.000	0.000	0.000	0.000
25.	1.051	0.167	0.000	0.000	0.000	0.000	0.000	0.000	0.000
30.	0.967	0.255	0.000	0.000	0.000	0.000	0.000	0.000	0.000
35.	0.869	0.281	0.066	0.000	0.000	0.000	0.000	0.000	0.000
40.	0.778	0.282	0.098	0.000	0.000	0.000	0.000	0.000	0.000
45.	0.698	0.272	0.112	0.033	0.000	0.000	0.000	0.000	0.000
50.	0.628	0.257	0.117	0.047	0.000	0.000	0.000	0.000	0.000
55.	0.568	0.242	0.117	0.055	0.019	0.000	0.000	0.000	0.000
60.	0.516	0.226	0.115	0.059	0.027	0.000	0.000	0.000	0.000
65.	0.472	0.211	0.111	0.061	0.031	0.012	0.000	0.000	0.000
70.	0.433	0.198	0.107	0.061	0.034	0.016	0.000	0.000	0.000
75.	0.398	0.185	0.102	0.060	0.035	0.019	0.008	0.000	0.000
80.	0.368	0.173	0.098	0.059	0.036	0.021	0.011	0.000	0.000
85.	0.342	0.163	0.093	0.057	0.036	0.022	0.013	0.006	0.000
90.	0.318	0.153	0.089	0.055	0.036	0.023	0.014	0.008	0.000
95.	0.297	0.144	0.084	0.053	0.035	0.023	0.015	0.009	0.004
100.	0.278	0.136	0.080	0.052	0.034	0.023	0.015	0.010	0.006
105.	0.261	0.129	0.077	0.050	0.034	0.023	0.016	0.010	0.006
110.	0.246	0.122	0.073	0.048	0.033	0.023	0.016	0.011	0.007
115.	0.232	0.116	0.070	0.046	0.032	0.022	0.016	0.011	0.008
120.	0.219	0.110	0.067	0.044	0.031	0.022	0.016	0.011	0.008
125.	0.208	0.105	0.064	0.043	0.030	0.021	0.016	0.011	0.008

Table IIA

Low ($E_{p'}^{min}$) and upper ($E_{p'}^{max}$) energy (MeV) of the recoiled protons arising in reaction $\gamma + p \to \gamma' + e^+e^- + p'$.

ω - incident photon energy (MeV)
ω' - scattered photon energy (MeV)
θ - scattering angle (degrees)
E_p^{Compt} - Compton recoiled proton energy (MeV)

$\theta = 60^0$

$\omega' = 29$, $E_p^{Compt} = 0.455$			$\omega' = 39$, $E_p^{Compt} = 0.828$			$\omega' = 49$, $E_p^{Compt} = 1.31$		
ω	$E_{p'}^{min}$	$E_{p'}^{max}$	ω	$E_{p'}^{min}$	$E_{p'}^{max}$	ω	$E_{p'}^{min}$	$E_{p'}^{max}$
31.	0.443	0.516	31.					
36.	0.374	0.816	36.					
41.	0.329	1.19	41.	0.827	0.875			
46.	0.296	1.65	46.	0.718	1.26			
51.	0.271	2.19	51.	0.647	1.70	52.	1.29	1.43
56.	0.253	2.81	56.	0.592	2.21	57.	1.16	1.88
61.	0.237	3.52	61.	0.548	2.81	62.	1.07	2.40
66.	0.224	4.30	66.	0.511	3.49	67.	0.988	2.99
71.	0.214	5.17	71.	0.482	4.24	72.	0.923	3.66
76.	0.205	6.11	76.	0.457	5.08	77.	0.869	4.41
81.	0.198	7.14	81.	0.436	5.99	82.	0.822	5.23
86.	0.192	8.23	86.	0.418	6.97	87.	0.783	6.13
91.	0.186	9.39	91.	0.402	8.03	92.	0.748	7.10
96.	0.182	10.6	96.	0.389	9.16	97.	0.719	8.14
101.	0.177	11.9	101.	0.377	10.4	102.	0.692	9.25
106.	0.174	13.3	106.	0.366	11.6	107.	0.669	10.4
111.	0.170	14.7	111.	0.357	13.0	112.	0.649	11.7
116.	0.168	16.2	116.	0.349	14.4	117.	0.630	13.0
121.	0.165	17.8	121.	0.341	15.8	122.	0.614	14.4
126.	0.162	19.4	126.	0.334	17.4	127.	0.599	15.8

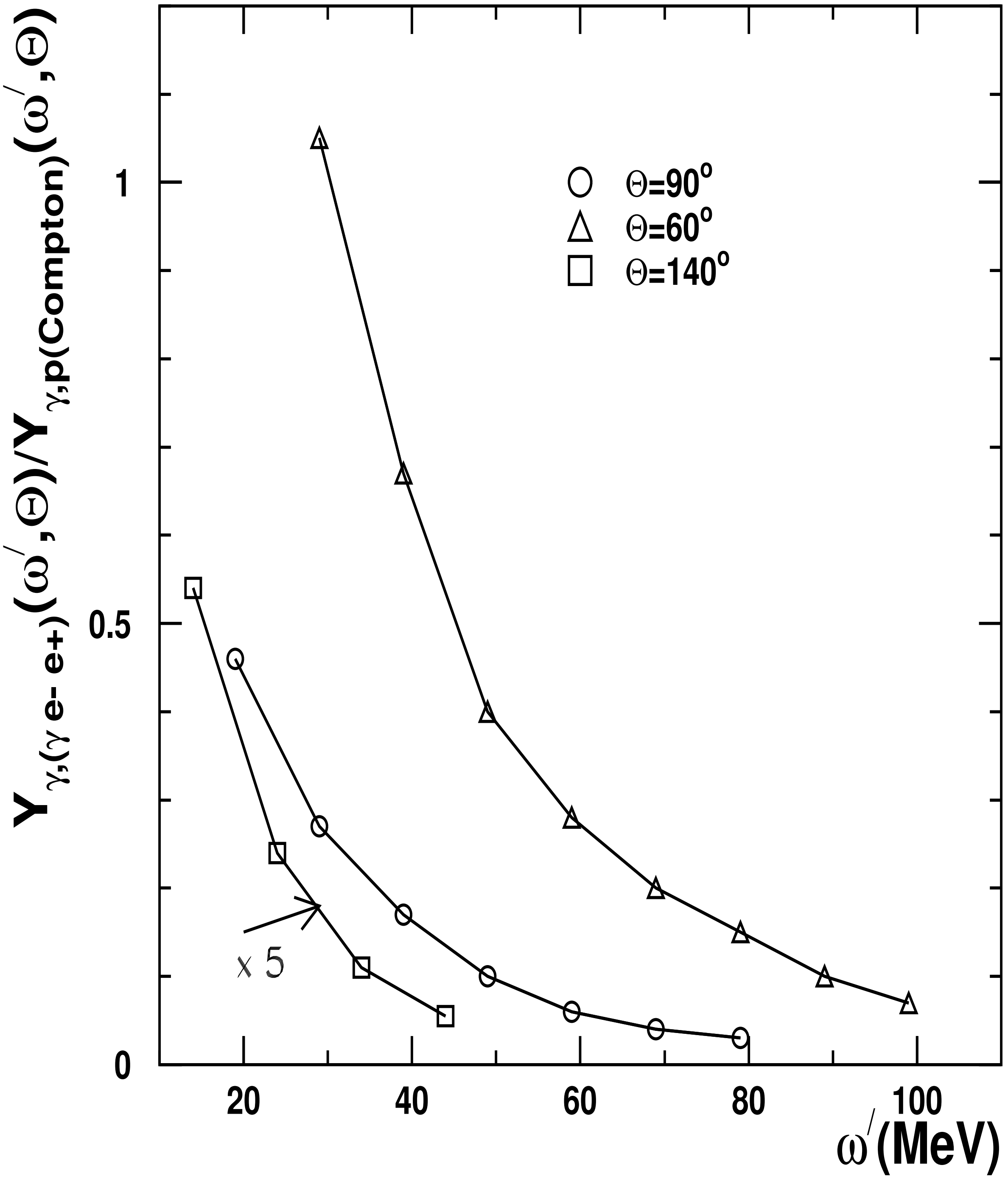

Fig.2A Ratio of the yield of inelastic scattered photons, $Y_{\gamma(\gamma',e^+e^-)}$, to the yield of elastic scattered photons, $Y_{\gamma p}$, integrated over the spectrum of incoming bremsstrahlung with $E_{\gamma\, max}$=130MeV.